Earth-Science Reviews 248 (2024) 104632

Contents lists available at ScienceDirect

Earth-Science Reviews

journal homepage: www.elsevier.com/locate/earscirev

Cryogenian–Cambrian tectono-sedimentary evolution, paleoclimate and environment effects, and formation of petroleum resources in the Tarim Block

Zhiyao Zhang [a,b,*], Guangyou Zhu [b,**], Weiyan Chen [b], Lin Wu [c,b], Rong Ren [b], Chuanlin Zhang [d]

[a] School of Earth Resources, China University of Geosciences, Wuhan 430074, China
[b] Research Institute of Petroleum Exploration and Development, PetroChina, Beijing 100083, China
[c] Institute of Geomechanics, Chinese Academy of Geological Sciences, Beijing 100081, China
[d] College of Oceanography, Hohai University, Nanjing 210093, China

ARTICLE INFO

Keywords:
Tectonic evolution
Sedimentary sequences
Paleoclimate
Glaciation
Petroleum source rock
Cryogenian–Cambrian
Tarim Block

ABSTRACT

Neoproterozoic tectonic evolution, magmatic activities, and sedimentary sequences are fundamental in understanding the transition from the dispersing of Rodinian continents to the assemblage of Gondwana and simultaneously supply crucial evidence for the global climate–environment change, i.e., from the Snowball Earth to a habitable Earth. In this contribution, we comprehensively synthesize the well-preserved Cryogenian–Cambrian sequences, multiple-phased magmatic activities, paleoclimate and environment in the Tarim Block of northwestern China to sketch a tectonic-sedimentary process from the breakup of Rodinia to the assemblage of Gondwana. We address the coupling between tectonic evolution process, glacial–interglacial cycles, paleoclimate and environment changes, and the formation of petroleum resources. In this study, we establish the stratigraphic frameworks in Kuruktag, Aksu, Tieklik areas in the northeast, northwest, and southwest of the Tarim Block, respectively. We review the differential geodynamic mechanisms and development processes of rifts in two discrete terranes, namely the North Tarim Terrane and South Tarim Terrane, of the Tarim Block to reconstruct the tectonic evolution process of Tarim during the Cryogenian–Cambrian interval and further decipher its control on the paleogeographic framework. The transition from extensional to compressional conditions during the early Cryogenian to Cambrian, combined with multiple phases of magmatic and glaciations, led to the three-stage evolution of sedimentary filling styles. We also document the evolution of glacial–interglacial cycles and how it impacts the paleoclimate and environment, sedimentary sequences, and the evolution and preservation of early life. The formation of organic-rich black mudstone/shale is attributed to the increasing nutrients in marine water and blooming of life in a warm-humid climate during interglacial periods; and thus, we propose the formation models of three favorable ancient petroleum source rocks in response to different tectono-sedimentary evolution stages and further estimate their quality, distribution, and resource potential. This review provides an improved understanding of the Cryogenian–Cambrian tectono-sedimentary evolution in the Tarim Block and its effects on the formation of ancient petroleum source rocks. It sheds insights into hydrocarbon accumulation theories and exploration strategies in ultra-deep ancient strata.

1. Introduction

Supercontinent events, including the assembly and breakup of Rodinia and the convergence of Gondwana, are critical during the Earth's evolution and have recorded the adjustments of lithospheric structures and significant changes during the Neoproterozoic (Li et al., 2008; Zhao et al., 2018). Major global plates also experienced distinct evolution during this period. This evolution has been reflected in different degrees in ancient China blocks, especially Tarim, as evidenced by thick Cryogenian–Ediacaran sedimentary sequences under rifting backgrounds and records of late Mesoproterozoic–early Neoproterozoic convergence, late Neoproterozoic breakup, and early Paleozoic tectonic

* Corresponding author at School of Earth Resources, China University of Geosciences, Wuhan 430074, China.
** Corresponding author.
E-mail addresses: geozzy@163.com (Z. Zhang), zhuguangyou@petrochina.com.cn (G. Zhu).

https://doi.org/10.1016/j.earscirev.2023.104632
Received 27 February 2023; Received in revised form 29 September 2023; Accepted 17 November 2023
Available online 25 November 2023
0012-8252/© 2023 Elsevier B.V. All rights reserved.

events preserved in Tarim and its surrounding orogenic belts (Chen et al., 2004; Xu et al., 2009, 2013a; Zhang et al., 2014a, 2014b, 2019a; Zhu et al., 2011, 2019, 2020c; Wen et al., 2018; Wu et al., 2020a, 2021b; Ren et al., 2020). Therefore, the Tarim Block and surrounding orogenic belts are crucial for studying the Neoproterozoic global tectono-sedimentary evolution. However, the relationship between the Tarim Block and the Precambrian supercontinent evolution and Neoproterozoic geodynamic background remains elusive.

According to multiphase Neoproterozoic igneous rock records in the periphery of Tarim (Li et al., 1998; Yang et al., 1997; Zhang et al., 2007a), including the 1048–933 Ma magmatic event (Shu et al., 2011), the 820–800 Ma ultramafic–mafic–carbonatite diamictites, mafic dyke swarms and granites (Zhang et al., 2007a; Zhu et al., 2008; Deng et al., 2008), the ca. 780–760 Ma ultramafic diamictites and mafic dyke swarms (Zhang et al., 2009a), and the ca. 650–630 Ma mafic dyke swarms (Zhang et al., 2009b). Given the early Neoproterozoic blueschist in the Aksu area, northwest Tarim Block, although its metamorphic age has not been well constrained, researchers proposed that this is genetically related to the assembly of Rodinia (Liou et al., 1996; Chen et al., 2004; Zhang et al., 2009b, 2009c; Zhu et al., 2011; Yong et al., 2013). However, due to the arc-signatures of Neoproterozoic igneous rocks, some have argued that such igneous rocks are related to the subduction of oceanic crust to the northern margin of the Tarim Block (Zhang et al., 2012b; Tang et al., 2016). Based on the newly discovered Neoproterozoic suture zone in the central Tarim Block (CTS) and the distinct Precambrian basements of the north and south Tarim Block, many researchers agree that it comprises two discrete terranes: North Tarim (NTT) and South Tarim (STT) (Fig. 1-a, Liou et al., 1996; Wu et al., 2012; Xu et al., 2013a; Zuza and Yin, 2017). They converged to the northern margin of Australia during 1.0–0.8 Ga and subsequently were subducted until 740 Ma (Fig. 1-a; Zhang et al., 2012b, 2016; Xu et al., 2005, 2009, 2013a, 2013b); thus, it is highly likely that Tarim was located on the northern margin of Rodinia (Zhang et al., 2007b; Zhao and Cawood, 2012; Zheng et al., 2013; Zhang et al., 2012b, 2013). Other researchers observed that the NTT and STT have distinct differences in the late Paleoproterozoic metamorphic events and continental growth characteristics and proposed that the two terranes merged during the assembly of the Rodinia supercontinent in the early–Middle Neoproterozoic (Guo et al., 2005; Xu et al., 2013a; Zhang et al., 2014a, 2014b; Wu et al., 2018a; Yang et al., 2018). Notably, the formation time of the CTS is still controversial with other opinions including the end of the Paleoproterozoic (Yang et al., 2018), late Mesoproterozoic (Li et al., 2005a), and Paleozoic (He et al., 2011; Li et al., 2014).

Therefore, the Neoproterozoic plate tectonic movements caused complex changes, tectonic evolution, and rift development within the Tarim Block and significantly affected the Tonian–Cambrian sedimentary sequences, primarily because of the changes in the paleoclimate and environment. Associated with plate tectonic activities, the dramatic and frequent changes of pCO_2 in the Neoproterozoic atmosphere led to the occurrence of multiphase glaciations from 750 Ma to 580 Ma (Brasier et al., 2000; Hoffman et al., 1998; Hoffman et al., 2002). Since the main body of the Rodinia supercontinent was near the equator during this period, intensive weathering of massive silicates caused the increasing consumption of CO_2 in the atmosphere, resulting in a thinner atmosphere, faster heat loss, and gradually strengthened the ice house effect. Consequently, four major glaciations occurred consecutively: Kaigas (750–741 Ma) (Frimmel et al., 1996; Macdonald et al., 2010; Zheng et al., 2007), Sturtian (720–660 Ma) (Brasier et al., 2000; Fanning and Link, 2004), Marinoan (654–635 Ma) (Halverson et al., 2004; Kendall et al., 2006), and Gaskiers (583–582 Ma) (Thompson and Bowring, 2000; Pu et al., 2016). The Snowball Earth hypothesis considers the Sturtian and Marinoan as comparable glacial events globally.

Glacier events globally have led to severe changes and disruption in the carbon and geochemical cycles of water bodies (Halverson et al.,

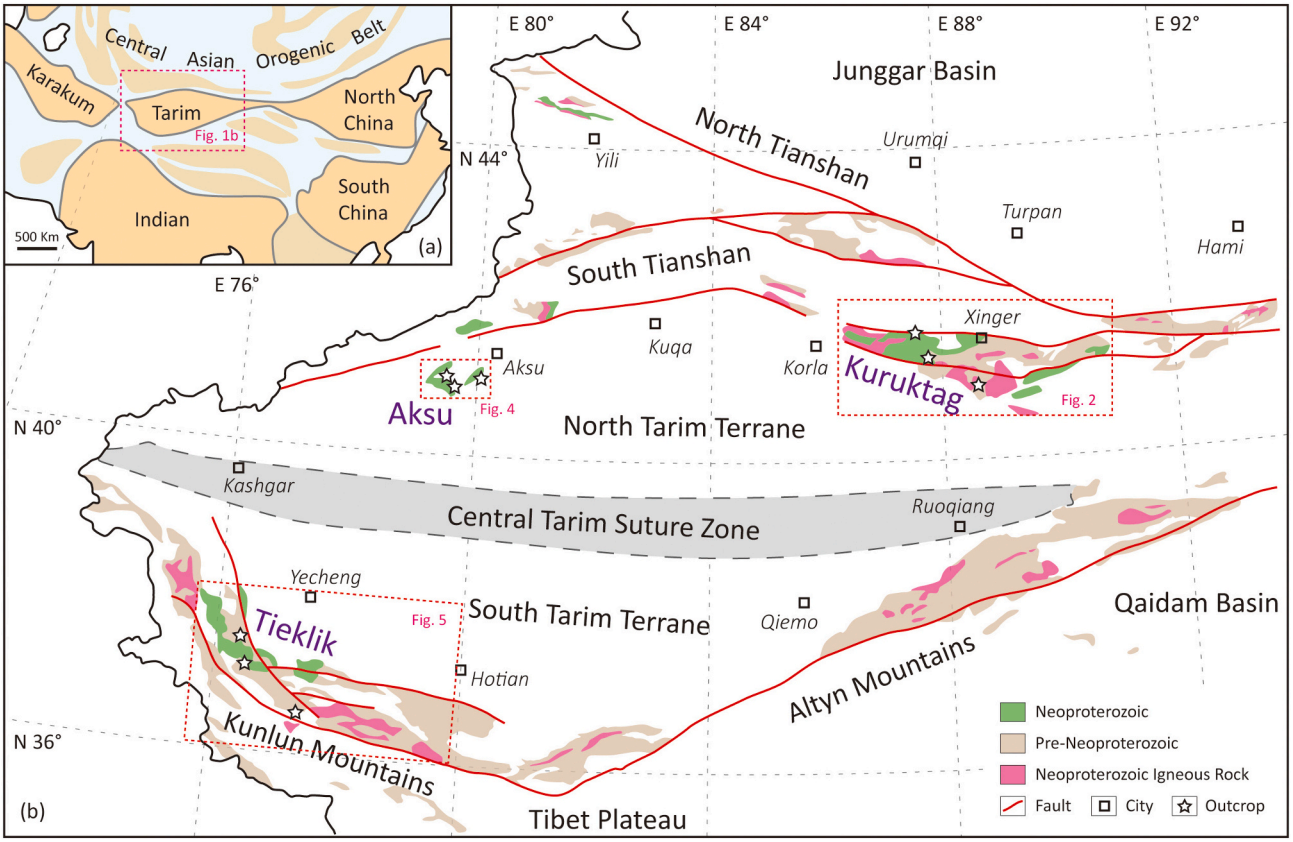

Fig. 1. Tectonic position (a) and distribution of the Neoproterozoic (b) of the Tarim Block.

2005; Yonkee et al., 2014); consequently, biological evolution entered crucial turning points during these periods (Hoffman et al., 1998; Love et al., 2009; Macdonald et al., 2010; Craig et al., 2013). Therefore, they are fundamental for understanding Neoproterozoic climate changes and oxidation events (Sahoo et al., 2012; Kunzmann et al., 2015; Wang et al., 2019; Wei et al., 2020) and for the isochronous correlation of global stratigraphy and studying sea-level fluctuations (Eyles and Januszczak, 2004; Le Heron et al., 2011). Volcanic eruptions (Hoffman et al., 1998) and gas hydrate leaks (Hurtgen et al., 2002) during the glacial periods led to the accumulation of large amounts of greenhouse gases, such as CO_2 and methane. Then, the global climate became warmer to terminate a glacial period, and the Earth entered an interglacial period. Therefore, the Earth experienced glacial and interglacial cycles in the Neoproterozoic era, developing different sedimentary sequences and assemblages (Allen and Etienne, 2008; Hoffman et al., 2017; Imbrie et al., 1992).

Several glacial–interglacial sedimentary records have been found in Kuruktag northeast and Aksu northwest of the Tarim Block (Ren et al., 2018; Zhu et al., 2020b). However, the paleogeographic backgrounds of the records are controversial, and the intrabasinal structural styles and evolution in corresponding periods noticeably affected the development and preservation of the glacial sedimentary sequences. Interpreting glacial–interglacial sedimentary and lithological assemblages is crucial for revealing the coupling effect of plate tectonics, paleoclimate, and environment and its control on lithofacies and paleogeography.

During the evolution of approximately 500 million years in the Neoproterozoic, the coevolution of complex geological and biological events in the lithosphere, hydrosphere, and atmosphere controlled the material basis for forming Neoproterozoic petroleum systems. Several Neoproterozoic hydrocarbon accumulation and potential zones have been discovered worldwide, and large and medium-sized oil and gas fields in some zones developed, showing broad exploration prospects of ancient oil and gas areas (Craig et al., 2009; Zhu et al., 2020a; Yan et al., 2022). Regarding the South China Craton (SCC) and Tarim Craton, the two major cratons in China, the SCC has achieved an in-depth understanding of the sequence framework during the rift period and the tectono-sedimentary-lithofacies-paleogeographic characteristics. Black carbonaceous shales with high organic matter abundance formed in the Datangpo and Doushantuo formations in the SCC, giving rise to Ediacaran large gas fields, such as Weiyuan and Anyue, that developed commercially at high efficiency (Xie et al., 2017; Qin et al., 2018; Wei et al., 2018). Ediacaran dark mudstone was found in the Tarim rift sequence in the same period as the SCC, where oil and gas of different degrees were found in outcrops and drilling wells. However, this sedimentary sequence has been poorly understood, and the Neoproterozoic basin–mountain setup and paleogeographic evolution model of Tarim have remained unclear, hindering the study of the Precambrian tectonic-climate–environment effect and oil/gas geology in the Tarim Basin.

In recent years, with the supplement of aeromagnetic, 3D seismic, drilling, and field data and the wide application of rock chronology, studies on the distribution and evolution of the Neoproterozoic in the Tarim Block have made preliminary progress. Based on the systematic review of previous studies, this study aims to answer two fundamental issues including: (a) the control of the internal and external tectonic evolution of the Tarim Block on the sedimentation, climate, environment, and paleogeography, and (b) the formation of petroleum resources under the evolution of paleoclimate and the environment. It is critical for revealing the tectono-sedimentary evolution of the Tarim Block during the Neoproterozoic, estimating the exploration potential of ancient strata, and seeking large-scale oil, gas, and resource replacement areas in the ultra-deep strata of the Tarim Basin.

2. Stratigraphic framework and characteristics in primary outcrops

The Tarim Block lies within the Eurasian Plate, bounded by the Tianshan Mountains to the north, West Kunlun Mountains to the southwest, and Altyn Mountains to the southeast. Cenozoic deserts cover most of the block, and the Neoproterozoic crops out primarily in Aksu in the northwest, Kuruktag in the northeast, and Tiekelik in the southwest Tarim Block (Fig. 1).

2.1. Kuruktag area

A complex pre-Cryogenian basement was observed in the Kuruktag outcrops, including, from old to young, the tonalite–trondhjemite–granodiorite (TTG) rock series of the Neo-Archean Tuoglakbrak Formation, regional metamorphic rocks, such as schist-gneiss of the Paleoproterozoic Xingditag Group, slightly metamorphosed clastic rocks of the Mesoproterozoic Yangjibrak Group, and the dolomite marbles and epimetamorphic clastic rocks of the Ai'erjigan and Neoproterozoic Pa'ergangtag groups (Zhang et al., 2011b; Zhu et al., 2020b).

A complete Cryogenian–Ediacaran succession is exposed in this site (Figs. 2 and 3). Overlying Tonian granite unconformably, the Cryogenian is thicker in the north and thinner in the south. It is also characterized by stronger volcanic activities and a primarily delta-shelf sedimentary system in the south, whereas weak volcanic activities and shore-continental shelf depositional system with characteristics of a rifting depocenter appear in the north. (Zhang et al., 2012a, 2012b; Shi et al., 2017; Wu et al., 2020a; Zhu et al., 2021a). From the bottom to the top, the Cryogenian comprises the Baiyisi (Nh_1b), Zhaobishan (Nh_2z), Altungal (Nh_2a), and Tereeken (Nh_3t) formations, primarily comprising fluvial-delta facies glutenite and dark mudstone of deep-water continental shelf facies above the massively thick volcanic rocks, intercalated with multiple layers of volcanic rocks and tillite. The mudstone beds have a total organic content (TOC) of over 1.0%. Three phases of Cryogenian glacial deposits were identified: Baiyisi, Altungal, and Tereeken, correlating with those in other continents (Li et al., 2008). Furthermore, interglacial deposits were preserved in the Zhaobishan Formation.

Overlying the Cryogenian unconformably, the Ediacaran comprises the Zhamokti (Z_1z), Yukengol (Z_1y), Shuiquan (Z_2s), and Hangelchaok (Z_2h) formations, from bottom to top. It inherits the characteristics of a delta sedimentary system in the south, while it is dominated by continental shelf facies in the north of Kuruktag. Unlike the sedimentary environment of the passive continental margin in NW and SW Tarim, a set of mixed shelf siltstone and mudstone assemblage and deep shelf dolomitic mudstone were successively deposited during the depression evolution stage of the aulacogen basin in NE Tarim. The differences in sedimentation between the north and south parts of Kuruktag diminished, and the carbonate content increased gradually during the late Ediacaran. Furthermore, tillite and glacial lacustrine deposits were observed in the Hangelchaok Formation at the top of the Ediacaran in the field outcrops, typically considered to be correlated with the Gaskier glaciation (Bowring et al., 2003; Yi et al., 2022).

The Cambrian comprises the Xishanbrak ($Є_1x$), Xidashan ($Є_1xd$), and Mohershan ($Є_1m$) formations, from bottom to top, and is a set of sediments dominated by bathyal–neritic facies. The bottom of the Xishanbrak Formation comprises yellowish-brown and grayish-black phosphorus-bearing silicalite and corresponds to the Cambrian global phosphorite sedimentary event. The lower part of this formation comprises gray-green mafic igneous rocks, and the middle and upper parts black silicalite. The Xidashan Formation comprises gray-grayish-black limestone and marl interbedded with shale, calcareous sandstone, and dolomitic limestone. The Mohershan Formation contains interbedded and argillaceous limestone, with black silicalite at the bottom.

2.2. Aksu area

In the Aksu area, the Precambrian was found in the Linkuanggou, Shiairik, Yuermeinak, and other outcrops (Fig. 4), and the Cryogenian forms an angular unconformable contact with a set of thick flysch

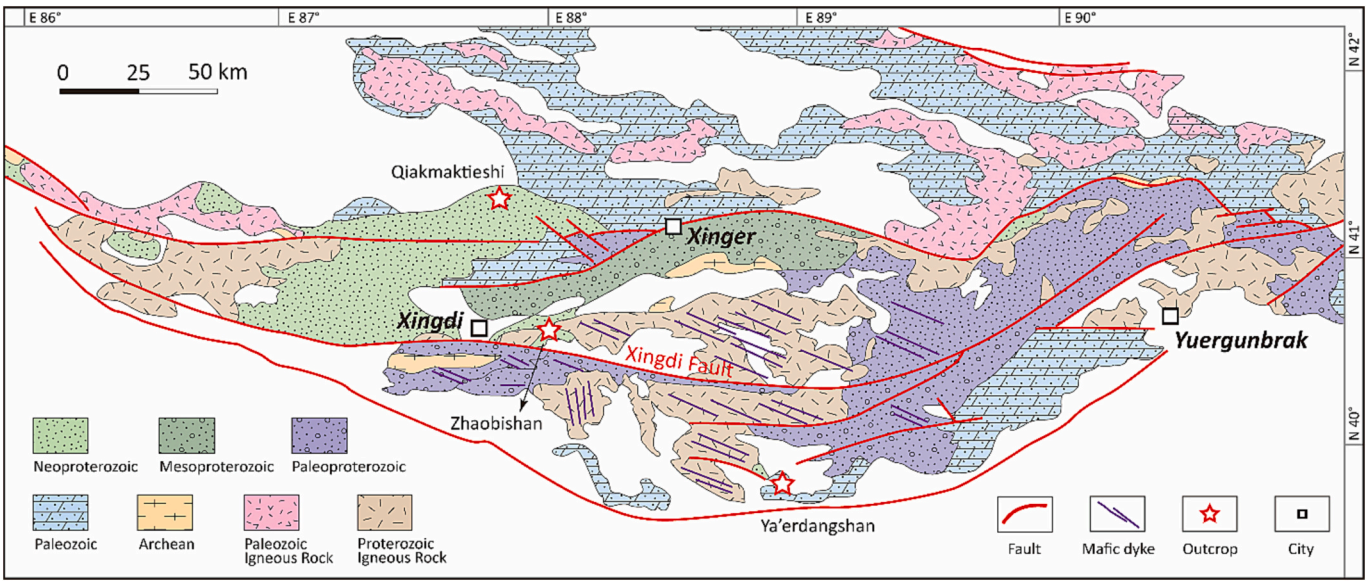

Fig. 2. Distribution of the Neoproterozoic in the Kuruktag area, northeast Tarim Block (after Zhang et al., 2012a, 2012b).

deposits of the underlying Xifangshan Formation (Nh_1x). The U-Pb ages of the detrital zircons from the Xifangshan Formation range between 860 and 840 Ma. From the bottom to the top, the Cryogenian comprises Dongqiao'enbrak Formation (Nh_2dq) tillite, Muyangtan Formation (Nh_2m) calcareous sandstone, Dongwu Formation (Nh_2dw) conglomerate, and Yuermeinak Formation (Nh_3y) continental tillite, reflecting the transition from deep-water mudstone to braided river sandstone and alluvial fan glutenite deposits (Wu et al., 2018a; Shen et al., 2022). In the field, Nh_3y and Nh_2dw form a micro-angular unconformable contact, and the Yuermeinak tillite can be correlated with Tereeken tillite in Kuruktag. Therefore, the Yuermeinak tillite in Aksu belongs to the Marinoan glacial period (Vandyk et al., 2019).

The Ediacaran here overlies the Cryogenian Yuermeinak Formation tillite unconformably, and in some sections, such as Shiairik, the Ediacaran overlaps unconformably on the Aksu Group greenschist basement (Wu et al., 2023; Zhang et al., 2022). The Ediacaran in northwest Tarim comprises the Sugetbrak (Z_1s) and Qigbrak (Z_2q) formations. The Z_1s transitions from alluvial fan-braided river facies glutenite and littoral–neritic facies sandstone and mudstone to tidal-flat facies gypsum-bearing sandy mudstone and algal dolomite from the bottom to the top, with wave ripple marks and pinnate cross-bedding developed (Wu et al., 2023; Zhang et al., 2022). The Z_2q primarily comprises a set of thick-bedded microbial and grain beach dolomite and has suffered weathering crust karstification at the top.

The Cambrian in Aksu is widely exposed and in parallel unconformable contact with dolomite at the top of the underlying Qigbrak Formation, with scouring surfaces and karst layers in between. The stratigraphy includes the Lower Cambrian Yuertusi ($Є_1y$), Xiao'erbrak ($Є_1x$), and Wusongger ($Є_1w$) formations, the Middle Cambrian Shailik ($Є_2s$) and Awatag ($Є_2a$) formations, and Upper Cambrian Xiaqiulitag ($Є_3x$) Formation, from bottom to top. The Yuertusi Formation has a lithological combination of silicalite–phosphorite black shale-carbonate formed in the middle-to-lower gentle slope environment controlled by upwelling currents. The black shale unit, with very high TOC (2%–6%, up to 16%), is a critical marine petroleum source rock in the Tarim Basin (Zhu et al., 2018) and has a small-scale sedimentary hiatus with thick dolomite of the overlying Xiao'erbrak Formation.

2.3. Tiekelik area

In Tiekelik, southwest Tarim, the Cryogenian–Ediacaran strata are primarily exposed along the Xinjiang–Tibet Highway in Yecheng (Zhang et al., 2019b; Zhu et al., 2020a; Fig. 5). Unconformably overlying the Tonian Sukurok Formation, the Cryogenian comprises basal conglomerate and siliceous mudstone of the Yalaguzi Formation (Nh_1y), tillite of the Bolong Formation (Nh_2b), mudstone of the Kelisi Formation (Nh_2k), and tillite of Yutang Formation (Nh_3y), from the bottom to the top. Nh_1y, corresponding to the Baiyisi and Zhaobishan formations in Kuruktag, is a set of deep-water continental shelf facies deposits. Nh_2b, corresponding to the lower member of the Altungal Formation in Kuruktag, represents the tillites formed in glacial marine and continental shelf facies. Nh_2k, corresponding to the upper member of the Altungal Formation, represents the deposits of shelf-littoral facies after glacial melting. Nh_3y, corresponding to the Tereeken Formation, comprises grayish-green siliceous and silty mudstones in the lower part and purplish-brown glacial mélange in the upper part, reflecting a new glacial event.

The Ediacaran in this area is in parallel unconformable contact with the underlying Cryogenian and is overlain by a Devonian–Carboniferous unconformity. It comprises the lower Kuerkak Formation (Z_1k) clastic rocks and the Kezisuhumu Formation (Z_2k) dolomites, representing a sedimentary sequence transitioning from shelf-littoral facies sandstone–siltstone to tidal-flat facies sandstone–mudstone and algal dolomite. Drilling and outcrop data have confirmed that the entire Tarim Block had a sedimentary framework of a platform to the west and a basin to the east during the Cambrian. Thus, Cambrian sediments are typically absent in the Tiekelik outcrop area (Han et al., 2020) and will not be further discussed.

3. Igneous activities, tectonic settings, and evolution

There is a noticeable E–W-trending aeromagnetic anomaly zone in the central Tarim Plate, frequently interpreted as the central suture zone (CTS) between the STT and NTT, and has been confirmed by the different characteristics of Precambrian basements in these two discrete terranes. However, opinions vary regarding when the STT and NTT converged and how the tectonic evolution occurred in the Tarim Block (Jia, 1999; Li et al., 2005b; Guo et al., 2005; Xu et al., 2013a; Zhai, 2013; Guan et al., 2017; Yang et al., 2018; Zhou et al., 2021; Wu et al., 2022a). A comprehensive study on igneous activities, rift formation mechanisms, and Cryogenian–Cambrian sedimentary sequences is essential to answer these questions.

The Tarim Block records five phases of igneous rock activities at 950–900 Ma, 850–780 Ma, 760–720 Ma, 670–610 Ma, and 540–470 Ma

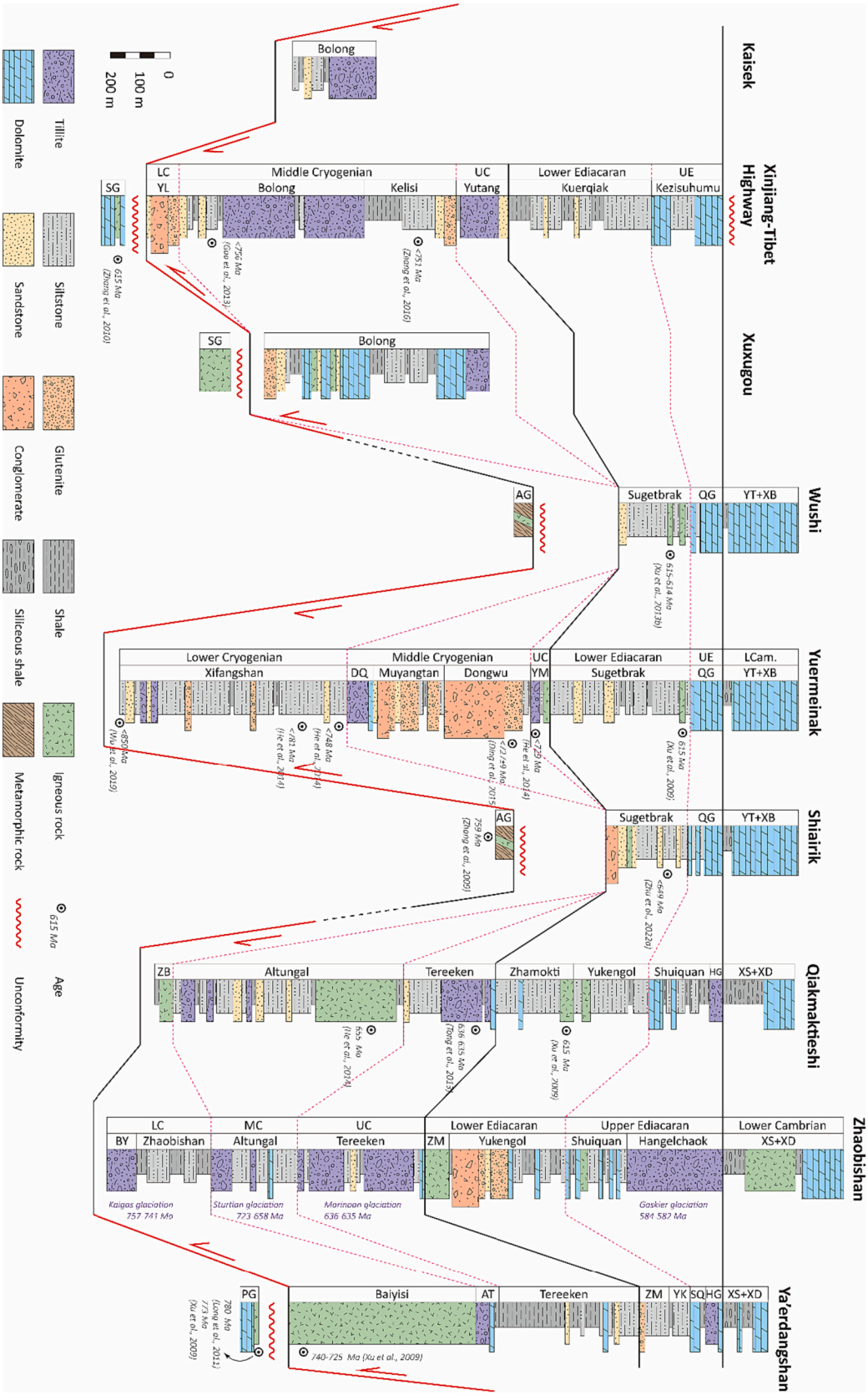

Fig. 3. Stratigraphic framework of typical Neoproterozoic outcrops across Tieklik, Aksu and Kuruktag areas in the Tarim Block (after Wu et al., 2018a; Zhu et al., 2020a). Note: AG, Aksu Group; AT, Altungal; DQ, Dongqiao'enbrak; HG, Hangelchaok; LC, lower Cryogenian; LCam, lower Cambrian; MC, middle Cryogenian; QG, Qigbrak; SG, Sukurok Group; SQ, Shuiquan; UC, upper Cryogenian; UE, upper Ediacaran; XB, Xiao'erbrak; XD, Xidashan; XS, Xishanbrak; YK, Yukengol; YL, Yalaguzi; YM, Yuermeinak; YT, Yuertusi; ZB, Zhaobishan; ZM, Zhamokti.

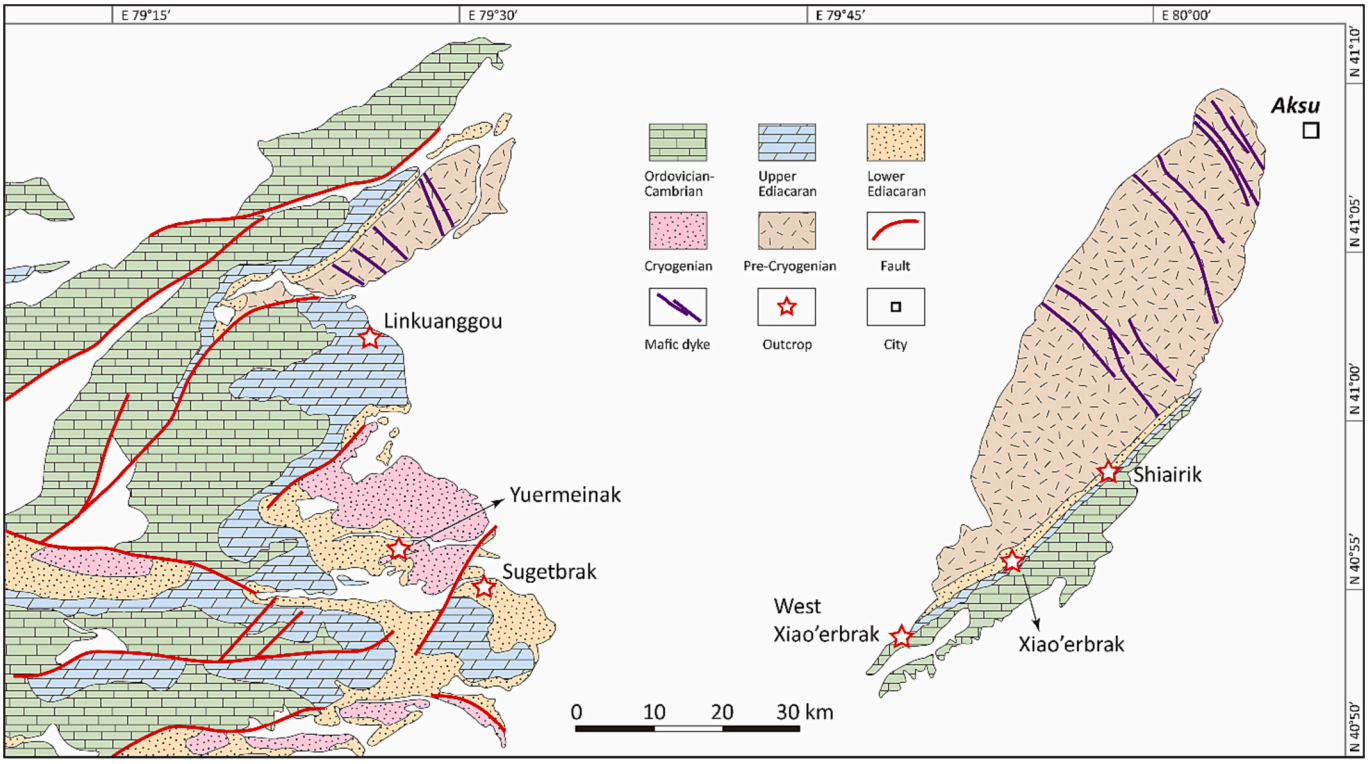

Fig. 4. Distribution of the Neoproterozoic in the Aksu area, northwest Tarim Block (after He et al., 2019b; Chen et al., 2020; Wu et al., 2022a).

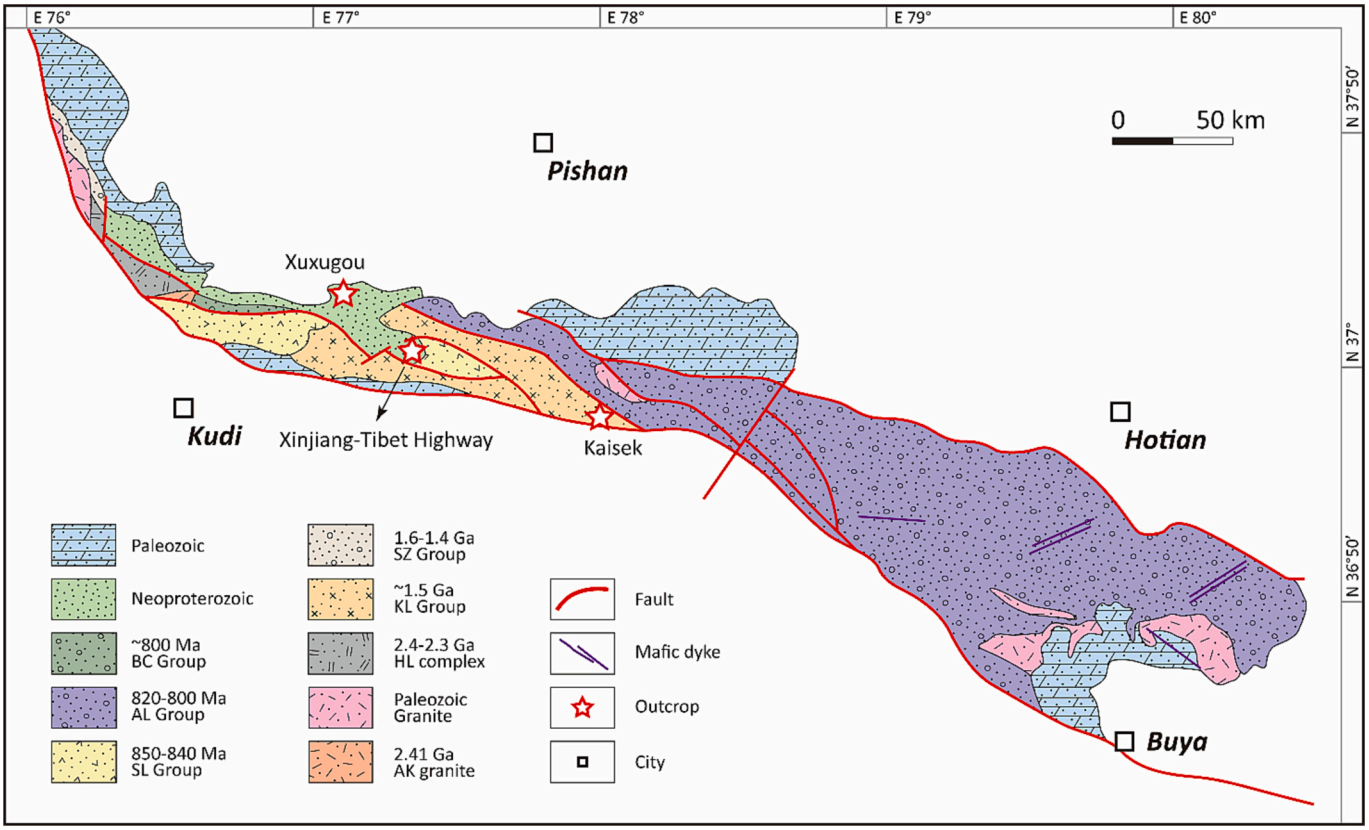

Fig. 5. Distribution of the Neoproterozoic in the Tieklik area, southwest Tarim Block (after Zhang et al., 2019a; Zhou et al., 2021).

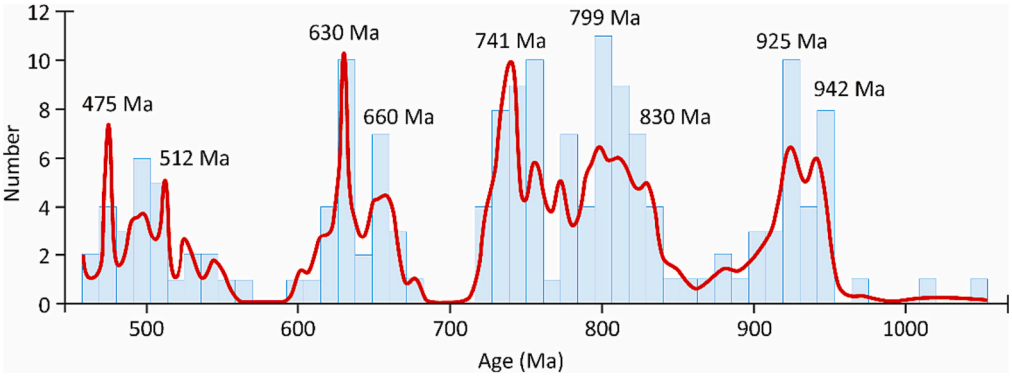

Fig. 6. Significant U-Pb age histogram of Neoproterozoic magmatic rocks in the Tarim Block (part of the data from Wu et al., 2020b; Zhu et al., 2021b and references therein).

during the Neoproterozoic–Cambrian (Zhang et al., 2019b, 2019c; Wu et al., 2018b, 2020b; Zhu et al., 2021b) (Fig. 6). In the spatial distribution, a minority of igneous activities at 950–900 Ma and 850–780 Ma occurred in the Altyn, Central Tianshan, and West Kunlun Mountains around the Tarim Block. Igneous activities during 760–740 Ma were more widely distributed. Those during 740–720 Ma correlate with the distribution of the Cryogenian rifts since 740 Ma, and those during 670–610 Ma gradually retreated to the north and northwest Tarim. The Cambrian ones were concentrated in the West Kunlun and Altyn Mountains. The Cryogenian–Cambrian strata contain various felsic and mafic magmatic rocks with similar trace element patterns (Zhang et al., 2017, 2019a; Wu et al., 2020b). The formation environments of most rock samples are interpreted as subduction-related volcanic arc and post-orogenic environments. The mafic rocks are primarily tholeiitic basalts with significant variations in geochemical properties, and their genesis is typically interpreted as intracontinental rift environments (Xu et al., 2009, 2013a; Zhang et al., 2013). However, the mafic–ultramafic intrusive rocks (820–735 Ma) have geochemical characteristics similar to basalts formed under subduction (Wu et al., 2020b; Zhou et al., 2022).

3.1. *Differences in igneous activities between STT and NTT*

STT and NTT have distinct differences in igneous records. The earliest Neoproterozoic igneous record in the STT is the basalt ~890 Ma in the lower Sailajiazitag Group. It is characterized by short time duration, huge thickness (>4600 m), and geochemical signatures of continental flood basalt (CFB) and is considered a fragment of the large igneous province of the early Neoproterozoic (Wang et al., 2014; Zhang et al., 2019b). The sedimentary assemblage and geochemical characteristics of basalts in the Upper Sailajiazitag Group (850–840 Ma) are of typical extensional setting of a back-arc basin (Yuan et al., 2004). The 802 Ma mafic dykes and minor Neoproterozoic juvenile basalts in the Xuxugou Formation have typical ocean–island basalt (OIB) geochemical characteristics (Zhang et al., 2010). However, the 802 Ma mafic dykes and 780 Ma bimodal intrusive series of the Kuda Complex have intraplate features, including gabbros and granites with OIB- and A-type geochemical characteristics.

Compared with the STT, the earliest Neoproterozoic igneous record in the NTT is the andesite ~900 Ma with arc-like geochemical signatures (He et al., 2019b). Furthermore, 820–800 Ma carbonatite–ultramafic complexes and granites, 780–760 Ma mafic dyke swarms, 740–735 Ma mafic intrusive rocks, bimodal intrusive complexes, and volcanic rocks in the lower Baiyisi Formation, and 635–615 Ma granites, mafic dykes, and basalts in the Sugetbrak Formation have also been found in Aksu (Xu et al., 2013b; Chen et al., 2020). The 820–800 Ma carbonatite–ultramafic complex is derived from the subcontinental lithosphere mantle (SCLM) in extensional tectonic settings (Zhang et al., 2007b; Ye et al., 2013). A mafic intrusion and numerous basic dykes representing the 780–760 Ma magmatism show subalkaline and tholeiitic features (Ni et al., 2018) (arc-like features) and can be derived from melt/fluid metasomatized lithospheric mantles (Zhang et al., 2013). The bimodal intrusive complex and volcanic rocks of the lower Baiyisi Formation around 740–735 Ma show geochemical characteristics transitioning from arc-like to intraplate features (Xu et al., 2009). The 635–615 Ma basalts in the Sugetbrak Formation in Aksu are much fewer than those in the previous phases of igneous activities and have alkaline characteristics and most characteristics of CFB (Xu et al., 2013b; Chen et al., 2020).

3.2. *Differential formation mechanism of rifts in STT and NTT*

Multiphases of Neoproterozoic–Cambrian magma along the periphery of Tarim region were formed in diverse environments, including the active continental margin and the Circum–Rodinia subduction system (Zhu et al., 2011; Ge et al., 2014; Tang et al., 2016; Wu et al., 2020b). According to the spatial differences of magmatic records and the latest data, the Tarim Block is at the northern margin of the Rodinia supercontinent, away from the center of the Rodinia mantle plume, bordering the northern part of the Australian Block to the south and facing the Pan-Rodinia Ocean to the north (Li et al., 2008, 2013; Fig. 7). STT and NTT have obvious differences in the formation mechanism of the rift. First, regarding the formation time, STT has 802–783 Ma mafic dyke swarms and bimodal magmatic rocks, representing the lower limit of the rift-opening time (Zhang et al., 2010). In NTT, mafic dyke intrusions of 773–759 Ma found in blueschist metamorphic basement and early granites indicate that the rifts began to be active and received overlying Cryogenian–Ediacaran sediments at least after 759 Ma (Zhang et al., 2009a; He et al., 2014). The rift-opening time in STT is earlier than that in NTT.

Regarding the dynamic background of the Neoproterozoic rifts, since STT was connected with Australia and located inside the Rodinia supercontinent, its extensional background was primarily caused by the upwelling of the super-mantle plume or the mantle plume within the plate and was affected by the relatively slight subduction of the supercontinent periphery. This result is confirmed by intraplate/intracontinental OIB-type features represented by the mafic dyke swarm and bimodal magmatic rocks (Zhang et al., 2010; Zhao et al., 2014). It is noteworthy that greenstone-facies metamorphism and compressional deformation have been recorded in the Ailiankat Group in the eastern Tiekelik area at 776–790 Ma, before the Cryogenian. This is probably because the stress condition of the STT changed from tension to compression due to the convergence of STT and NTT, which further induced the formation of a foreland basin overlying the pre-existing arc sequences (Long et al., 2019; Ye and Zhang, 2020). However, Cryogenian mafic dyke swarms and bimodal volcanic rocks in Aksu and Kuruktag at the northern margin of the NTT have noticeable subduction

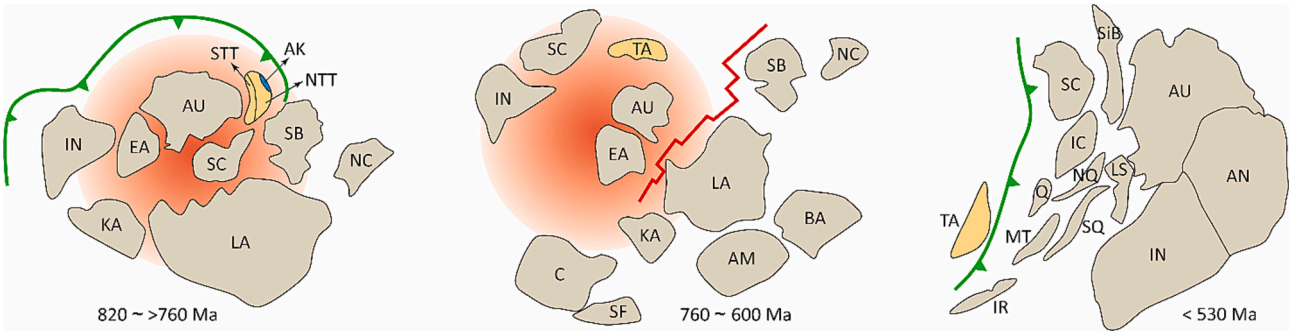

Fig. 7. The role of the Tarim Block during the Neoproterozoic (after Zhu et al., 2021a; see details in sections 3.2 & 3.3). Note: AK, Aksu area; AM, Amazon; AN, Antarctica; AU, Australia; BA, Baltica; C, Congo; EA, eastern Antarctica; IC, Indochina; IN, India; IR, Iran; KA, Kalahari; LA, Laurentia; LS, Lhasa; MT, Mazar terrane-Tianshuihai terrane; NC, North China; NQ, North Qiangtang; NTT, North Tarim Terrane; Q, Qaidam; SB, Siberia; SC, South China; SF, São Francisco; SiB, Sibumasu; SQ, South Qiangtang; STT, South Tarim Terrane; TA, Tarim Block.

features (Xu et al., 2005; Zhang et al., 2009a), closely related to the fact that NTT was at the outer edge of the Rodinia supercontinent and would inevitably have been affected by the subduction zone around Rodinia for the duration. Furthermore, the Cryogenian in the NTT lacks typical high-temperature products of a mantle plume, such as OIB-type basalt or high-Mg basalt, and the Baiyisi Formation sandstones have geochemical characteristics of active continental margin clastic rock (Zhang et al., 2011a). All these features indicate that NTT had a back-arc rift basin model in the Cryogenian period. However, several sets of igneous rocks from the Ediacaran to early Cambrian differ considerably from the

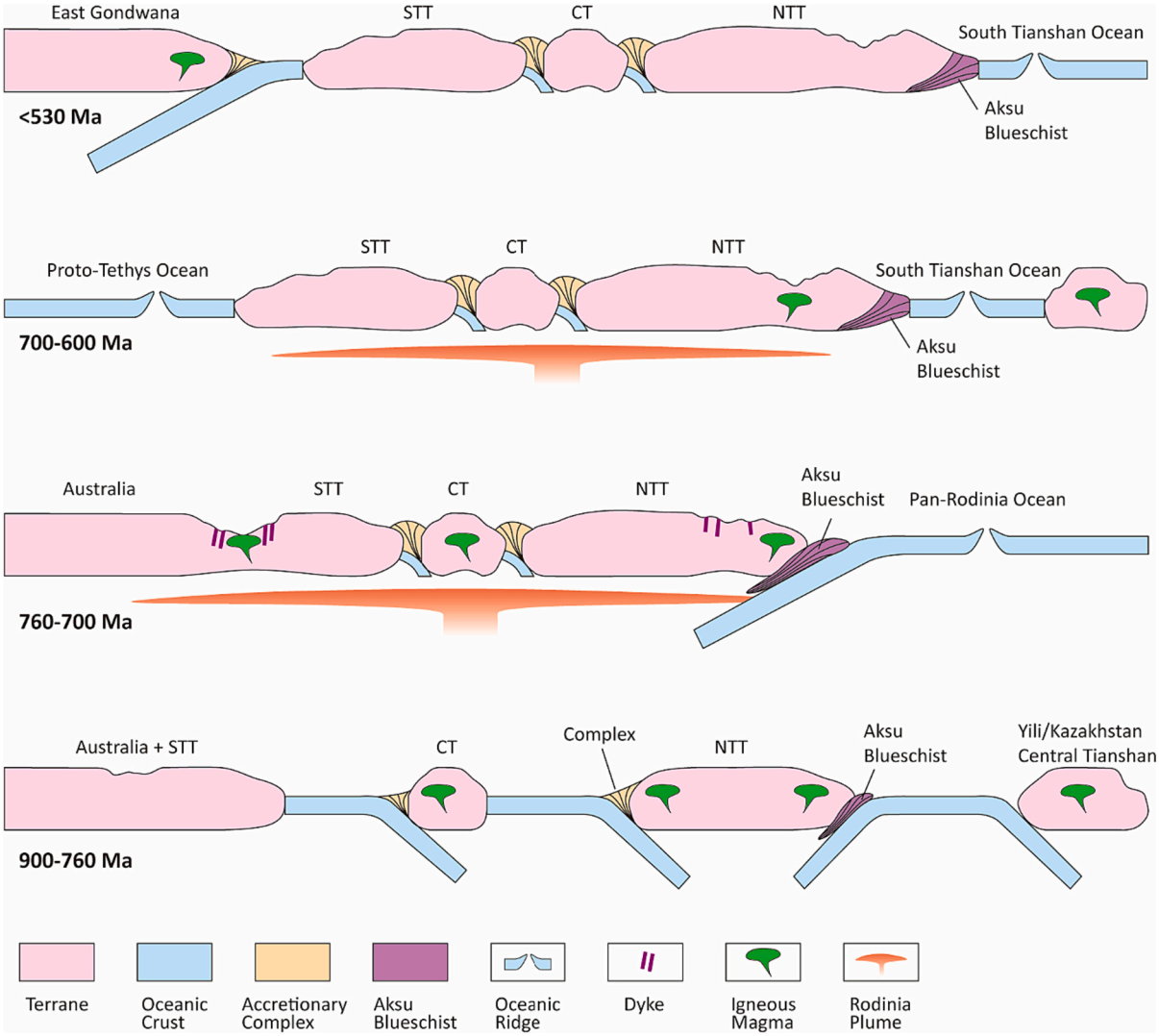

Fig. 8. Tectonic evolution of the Tarim Block and its peripheral regions during the Neoproterozoic. Note: CT, Central Tarim terrane; NTT, North Tarim terrane; STT, South Tarim terrane.

Cryogenian mafic dykes and bimodal magmatic rocks in geochemical characteristics. All show OIB characteristics, reflecting the weakening and the gradual replacement of subduction by the mantle plume activity in this period.

3.3. Tectonic evolution of the Tarim Block during the Neoproterozoic

According to Columbia reconstruction (Zhang et al., 2012a) and Mesoproterozoic sedimentary characteristics, igneous activity sequences, and metamorphism in the STT and NTT, the STT might be a continental fragment that separated and drifted from the western margin of the Congo Craton. The NTT is a continental fragment separated from the northern Sino-Indian Craton during the breakup of Colombia (Zhai et al., 2011; Zhao et al., 2011; Wang et al., 2020b). The STT was separated and drifted from the Congo due to the mantle plume effect. Along with the convergence of the Rodinia supercontinent, and due to the subduction of the northern margin of NTT, the NTT and STT began to converge along the central Tarim terrane. The time was estimated at around 890 Ma by I-type granites (Li et al., 2005b) and at ca. 760 Ma by zircon SHRIMP U-Pb age of core samples from wells drilled in the central Tarim terrane (Wu et al., 2009). The final convergence time might have lasted until after 780 Ma (Shu et al., 2011; He et al., 2013; Yong et al., 2013; Zhang et al., 2014a). The detrital zircons from the Upper Sailajiazitag (840 Ma) and Ailiankat formations (800 Ma) were formed in a convergence–collision environment, corresponding to the development of a back-arc basin around 840 Ma and the formation of the Ailiankat Formation flysch-like meta-graywacke around 800 Ma in STT, indicating that it is related to the compression condition in the foreland basin formed due to the convergence of STT and NTT (Xu et al., 2013a, 2013b; Zhang et al., 2016; Ye and Zhang, 2020, Wu et al., 2021a).

Based on the metamorphism of the Aksu Group blueschist and the prolonged arc-affinity igneous activities from 900 to 740 Ma, the subduction of the northern margin of NTT lasted until before 760 Ma. The ocean between the Tarim and Yili-Kazakhstan-Central Tianshan blocks closed, and the two blocks collided during the Middle Neoproterozoic (Fig. 8) (Zhang et al., 2009a, 2014a, 2014b; Yong et al., 2013; He et al., 2021; Wu et al., 2022b, 2023). The interaction between the Rodinia mantle plume and plate subduction during this period can explain the formation of numerous mafic dykes with arc-like characteristics (Li et al., 2008, 2009). The STT and NTT had wide differences in rift characteristics and development mechanisms at this stage. Affected by the activities of the global super-mantle plume, rift basins started to take shape in the STT in the Early Cryogenian, sharing the distribution and evolution characteristics of typical mantle plume rifts. Furthermore, the Pan-Rodinia oceanic subduction system primarily controlled the NTT (Zhang et al., 2009a, 2014b), and the back-arc extension caused by plate subduction was weak in this period; therefore, the rift in the NTT had not opened. The back-arc extension in the NTT peaked in the Early Cryogenian (after 720 Ma), and the Baiyisi bimodal volcanic rocks marked the opening of the back-arc rift basin, which was long and narrow in an E–W strike.

It is inferred from the Cryogenian passive continental margin sedimentary sequences that the Tarim Block started to separate from the Rodinia supercontinent at the beginning of the Cryogenian, characterized by large-scale and widespread marine sedimentary rocks and organic-rich mudstones deposited in this period (for more details about the sedimentary characteristics, see section 4; Xu et al., 2009; Chen et al., 2020; Zhu et al., 2020c). During the separation process, a series of Neoproterozoic rifts were formed, and igneous events representing continental breakup were found in Tarim, including bimodal volcanic rocks widely developed around 740–735 Ma (Xu et al., 2009, 2013b; Zhang et al., 2011b) and the widespread magmatic events around 650–635 Ma (Long et al., 2011). The upwelling of mantle magma during continental disintegration caused them both. During the Ediacaran, the subduction belt in the north of the Tarim Block continued to shift toward the ocean, the back-arc extension gradually weakened, as evidenced by the gradually decreasing magmatic events and igneous records (Xu et al., 2013a, 2013b; Chen et al., 2020; Zhang et al., 2012b). However, the extension activity was too weak to form obvious rift structures like those in the Cryogenian. Instead, the Tarim Block entered a depression stage and further evolved into a passive continental margin environment (Cui et al., 2016; Shi et al., 2016; Cai et al., 2021). In the late Neoproterozoic, the Tarim Block gradually dispersed from the Rodinia supercontinent and moved toward low latitudes. Finally, it was entirely independent, with a passive continental margin background forming around the Tarim Basin (Li et al., 2008). As shown in a S-N direction seismic profile across the Tarim Block (Fig. 9), the Cryogenian is limitedly distributed in the rifts, while the Ediacaran formed during the depression stage has a wider distribution. Comparingly, the Cambrian covers the widest distribution due to the global transgression at that time.

4. Glacial–interglacial cycles and their paleoclimate and environmental effects

The Neoproterozoic glacial records and the evolution of glacial–interglacial cycles globally are significant for revealing climate–environment evolution, conducting stratigraphic isochronal correlation, and deciphering the preservation mechanisms of organic matters (Sahoo et al., 2012; Kunzmann et al., 2015; Eyles and Januszczak, 2004; Le Heron et al., 2011). Multiple glacial deposits were found in the periphery of Tarim, especially in Kuruktag in northeast Tarim, probably the only section globally with four sets of Neoproterozoic tillites and five sets of volcanic rocks cropping out (Fig. 3), where the earliest glacial occurred in the Early Cryogenian. Kuruktag was in a continental drift background in this period and primarily had glacial marine and interglacial neritic facies deposits associated with some volcanic eruption products. The lower part of the Baiyisi Formation has a 158 m thick tillite conglomerate unit with noticeable tillite characteristics, such as drop-stone. Therefore, it is regarded as the first phase of the Neoproterozoic glaciers in Kuruktag, corresponding to the Kaigas glacial period of the Kalahari Craton in southern Namibia (Zhou et al., 2004; Xu et al., 2005, 2009). Volcanic rocks at the lower part of the Baiyisi Formation are 740 ± 7 Ma, and those at the top are 725 ± 10 Ma (Xu et al., 2009).

Two sets of volcanic rocks in the upper part of the Altungal Formation have U-Pb ages of 655.9 ± 4.4 Ma and 654 ± 10 Ma, providing accurate ages for the tillite of this period. The Altungal glaciation is the second glacier phase in the Tarim Plate, and the cap carbonate rock samples above the tillite have $\delta^{13}C$ values of −7‰ to −2 ‰, similar to those of the Australian Cryogenian Tindelphina Formation (Giddings and Wallace, 2009), indicating their comparability. Therefore, it is believed that the Altungal glaciation corresponds to the Qiao'enbrak glacier in Aksu, the Bolong glacier in Tieklik, the Tiesi'ao, Chang'an, and Fulu glaciers (750–670 Ma) in South China, and the Sturtian glaciation in Australia (Zhou et al., 2004; Liu et al., 2015).

The black mudstone and sandstone in the lower member of the Tereeken Formation are typical interglacial deposits formed between two glacial periods (Luo et al., 2016; Xu et al., 2009) and a crucial sign that the Tarim Block entered the interglacial period after the end of the Sturtian glaciation, representing the rapid transition of the Earth from an extremely cold Snowball Earth to a warm environment. This rock unit is approximately 300 m thick and primarily comprises black shale. However, the upper member of the Tereeken Formation, approximately 440 m thick, comprises interbedded gray fine-grained lithic sandstone and grayish-black siltstone. Furthermore, this member of the Tereeken Formation has tillite developed, which can be compared with the Yuermeinak glacier in Aksu, the Yutang glacier in Yecheng, southwestern Tarim, the Nantuo glacier in South China, and the Marinoan glacier in Australia (Gao and Cheng, 1984; Gao et al., 2013). The Tereeken Formation is in unconformable contact with the Ediacaran Zhamokti Formation, and the andesite samples from the top of the Zhamokti

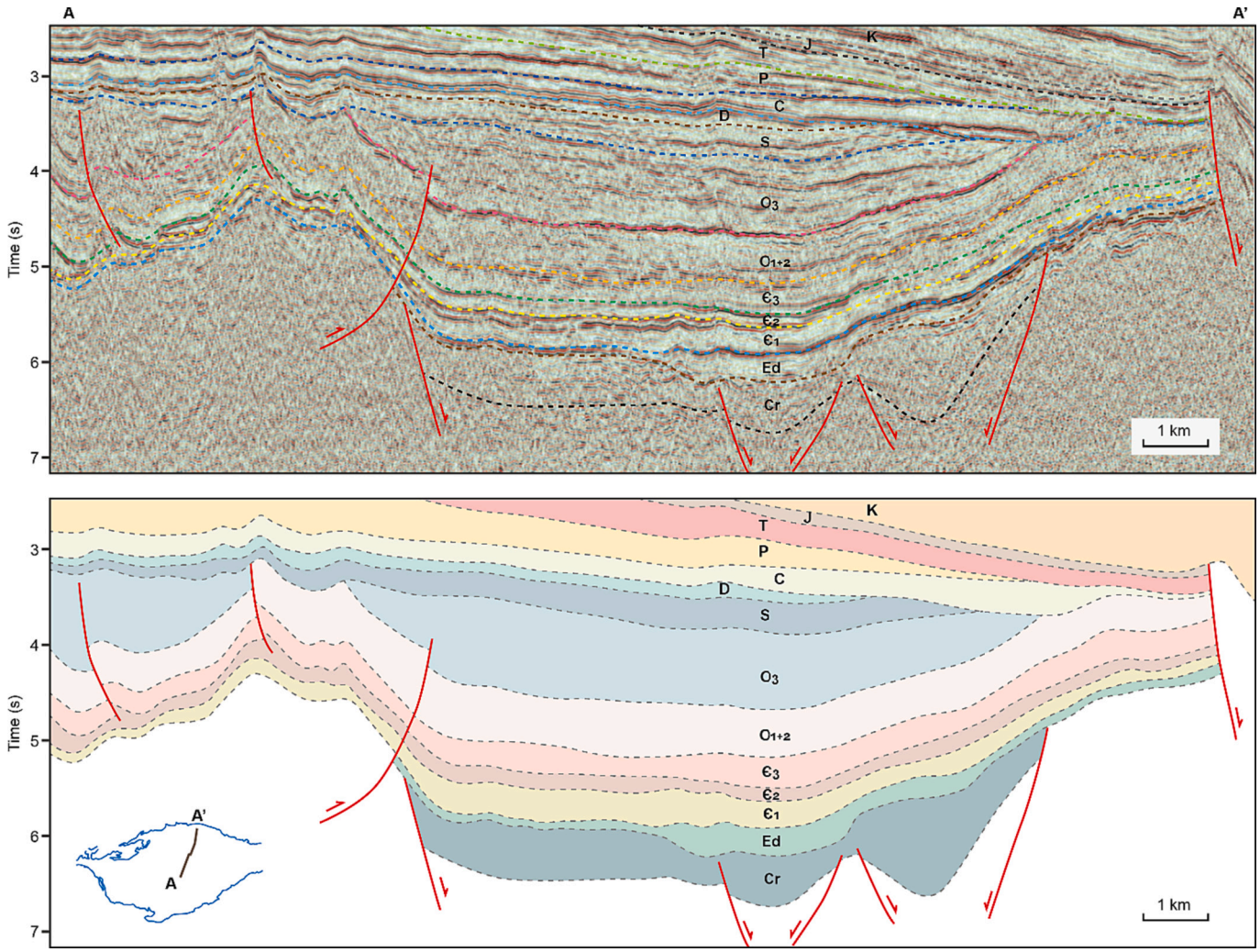

Fig. 9. S-N direction seismic profile across the Tarim Block (a) and its interpretation (b) showing the stratigraphic framework of the Tarim Block. Note: Cr, Cryogenian; Ed, Ediacaran; Є, Cambrian; O, Ordovician; S, Silurian; D, Devonian; C, Carboniferous; P, Permian; T, Triassic; J, Jurassic; K, Cretaceous.

Formation in the Xishankou section have a dated age of ~615 Ma (Xu et al., 2009; He et al., 2014), defining the age of the formation. Therefore, the lower member of the Tereeken Formation deposited during 654–635 Ma is a set of interglacial deposits, corresponding to the Cryogenian Datangpo Formation in South China.

The lithology of the Tereeken Formation has a noticeable response to the sedimentary environment changes. Gray-black and black shale dominate the lower member of the Tereeken Formation, representing the deep-water-reducing environment after the end of the glacial period of the Altungal Formation. The middle member comprises yellowish-green thin- to medium-bedded mudstone intercalated with dark gray-grayish-black thin- to medium-bedded siltstone, lithic sandstone, and brownish-gray thin-bedded dolomite. Such change in rock granularity is a response to the Pan-African tectonic movement which caused the regional uplift in the Kuruktag area, and the subsequent shallowing of sedimentary water body and the involvement of some terrigenous clastic materials in the sedimentation (Eyles and Januszczak, 2004; He et al., 2014; Scheller et al., 2018). The upper member comprises yellow-green, gray-grayish-black thin- to medium-bedded, fine-grained lithic sandstone and grayish-black thin-medium interbeds of siltstone because at the end of the Tereeken Formation, the Marinoan glacial period occurred, and the deposition of sandstone and mudstone sequences in the oxidizing environment peaked. The upper member of the Tereeken Formation in the north Kuruktag is dominated by marine ice-rafting, including subglacial and protoglacial deposits, where the deposits of the glacial period are thick. However, the upper Tereeken Formation in the south Kuruktag has thinner tillite deposits, primarily comprising mudstone, silty mudstone, and sandstone interbeds, with clasts coarsening from the bottom to the top and cap carbonate sediments locally (Turner, 2010).

The fourth glacial period in Kuruktag occurred during the late depositional period of the Ediacaran Hangelchaok Formation. During this period, the sedimentary difference between the north and south Kuruktag gradually diminished, and carbonate rocks increased proportionally. Tillite and glacial lake deposits of this period can be seen in the field. This glacier was found only in Kuruktag rather than in the northwest and southwest Tarim. With no igneous rocks around the tillite, it is impossible to tell its accurate age. However, according to the andesite at the top of the Zhamokti formation, the tillite age can be defined as 615–542 Ma. Furthermore, the carbonate samples from the top of Hangelchaok have a negative excursion of $\delta^{13}C$ (−11‰ to −4‰) and δO^{18} (−6.8‰ to −2.2‰), tallying with the characteristics of the C-O isotopic composition of cap carbonates formed after the glacial period (Zhu et al., 2020b). Currently, records of Ediacaran glaciers and their age data are few. One example is the Squantum diamictite in North America with an age of 595 ± 5 Ma (Thompson and Bowring, 2000), which is similar in age to the Hangelchaok tillite. It is believed that they correspond to the Gaskier glacier globally and the Luoquan glacier in North China (Zhao and Zheng, 2010).

The development of large-scale glaciers significantly affects the

paleoclimate and environment, especially the temperature, further affecting the activity of early life. Geochemical indicators of glacial and interglacial sediments can illustrate the response of paleoclimate–environment to glacial–interglacial cycles. For example, the chemical alteration index (CIA) ($Al_2O_3/(Al_2O_3 + CaO + Na_2O + K_2O)$), where CaO represents only the CaO in silicates and must be corrected according to McLennan (1993), can indicate the sedimentary environment and climate conditions accurately. CIAs between 50 and 65 reflect a low degree of chemical weathering in cold-dry climates, between 65 and 85 reflect a moderate degree in warm-humid climates, and between 85 and 100 represent intense weathering under hot and humid conditions (Nesbitt and Young, 1982; Wang et al., 2020a). The CIAs of the Cryogenian–Ediacaran glacial and interglacial deposits in Kuruktag have noticeable cyclic features. The CIAs of Baiyisi, Altungal, and top Tereeken deposits developed during the glacial period are 51–56, 48–62, and 49–52, respectively, indicating three periods of cold and dry climate. However, the CIAs of the Zhaobishan and middle and lower Tereeken and Shuiquan interglacial deposits increase significantly (approximately 60, 73, and 65, respectively), reflecting warm and humid sedimentary environments following the end of the glacial periods with the ice and snow melted and higher temperatures. The results corroborate that under the drive of multiphase Cryogenian–Ediacaran glacial events, cold and warm climates alternated (Xiao et al., 2004; Xu et al., 2005; Zhu et al., 2020b).

The $^{87}Sr/^{86}Sr$ of cap carbonates is frequently used to trace the terrestrial weathering source and sea-level changes. $^{87}Sr/^{86}Sr$ records of the Neoproterozoic cap carbonate samples are primarily between 0.7090 and 0.7130, slightly higher than the average value of late Neoproterozoic seawater (0.7072–0.7080) (Halverson and Hurtgen, 2007; Sawaki et al., 2010; Peng et al., 2011), which might be due to the additional ^{87}Sr input during the deposition of cap carbonates. The average $^{87}Sr/^{86}Sr$ values of three sets of cap carbonates of the Baiyisi, Altungal, and Hangelchaok formations in Kuruktag are 0.7121, 0.7110, and 0.7105, respectively, consistent with values previously reported. Combined with the climatic and environmental conditions reflected in CIA data during this period, the reason for the high $^{87}Sr/^{86}Sr$ ratios of these three sets of carbonate rocks is the greenhouse effect following the end of the corresponding glacial periods. In these periods, with the rapid increase in temperature and humidity globally, continental weathering became stronger. Hence, the terrigenous ^{87}Sr increased and was carried into the ocean by surface water, resulting in the $^{87}Sr/^{86}Sr$ anomaly of seawater. Furthermore, stronger continental weathering and increasingly abundant surface water also brought more nutrients into the ocean, rapidly increasing oceanic productivity. The organic-rich dark shale unit of the lower Tereeken Formation is the best response to interglacial climate change, confirming that the warm-humid environment followed the end of the glacial period and increasing sea level led to the recovery of paleoproductivity in the ocean.

5. Evolution of paleogeography and sedimentary environments

Tectonic movements, glacial periods, paleogeomorphology, and thermal events affect Neoproterozoic deposits globally, and thus, the sedimentary assemblage records vary significantly in different regions (Hoffman et al., 2017). Specifically, regional structural characteristics and the evolution of multiphase glacial–interglacial cycles significantly affect the characteristics of sedimentary assemblages. Tectonic dynamic backgrounds and pre-existing structural forms control the accommodation space for sediment transport and accumulation and, in turn, determine the characteristics of the sedimentary filling (Gao et al., 2013; Wang et al., 2004). During the glacial period, glaciation can result in large-scale in situ deposition, form tillite and cap carbonates with special structures, such as drop-stones and glacial scratches, and modify the original landform, affecting the subsequent deposition.

5.1. Early Cryogenian

Affected by the upwelling of the super-mantle plume in the Early Cryogenian, the Tarim Block gradually separated from the Australia Block and away from the Rodinia supercontinent and drifted to the south (Xu et al., 2009; Chen et al., 2020). Furthermore, it rotated counterclockwise (Zhou et al., 2012). The entire Tarim Block was in an extensional environment, with active volcanic activities related to continental rifts (Zhang et al., 2014a). The rifts in the basin were separated by bulges and had a strong segmentation effect, giving rise to several isolated rifting centers (He et al., 2019a, 2023) (Fig. 10-a). The Cryogenian is limitedly deposited in these rifting centers as evidenced by the basin-scale seismic profile (Fig. 9). The rifts in the NTT were mostly in a WNW strike, whereas those in the STT in a ENE strike.

During this period, the littoral–neritic sea dominated the sedimentary environment in the basin, and several volcano-sedimentary cycles developed. Large-scale rift-related bimodal volcanic rocks with ages of 755–740 Ma were formed after the initiation of the rift basins and they were discovered in the Ya'erdangshan area and Well Tong1 in the northeast of Tarim (Xu et al., 2005, 2013b). They became local volcanic eruption centers and massively thick basalts quickly accumulated there due to strong volcanic activities, forming volcanic rock highlands as major provenances (Wang and Li, 2003; Wu et al., 2018a). While in the Bachu area, volcanic rocks were drilled just below the Cambrian carbonates, and they were suggested to have erupted in an intracontinental rift settings (Shi et al., 2017). Since the rifts were close to the provenances, they were rapidly filled with deep-sea rift sediments dominated by gray-green/purplish-red pyroclastic and clastic rocks, with a limited distribution range but massive thickness (Fig. 11). Between the rift centers and the ancient land, transitional fine clastic rocks of neritic–littoral facies with signature sedimentary structures, such as cross-bedding and hummocky cross-bedding of wave origin formed due to the rapid transgression of seawater.

5.2. Late Cryogenian–Early Ediacaran

From the Late Cryogenian to the Early Ediacaran, the Tarim Plate was still in an extensional tectonic setting, but the extensional action was significantly weaker than in the Early Cryogenian. The rift basin in the NTT continued to develop with local volcanic rocks erupted in the Qiakmaktieshi area and wells Fang1 and He4 (Fig. 10-b). Tectonic uplifting resulted in the denudation and formation of unconformities in multiple areas of the plate. The unconformities varied in type in different parts of the basin. For example, the Ediacaran overlies the Cryogenian in parallel unconformity at the subsidence center of a rift. However, in the slope area of a rift or step-fault zone dominated by a continental shelf-delta fan-delta sedimentary system, the Ediacaran gradually overlaps on the Cryogenian in an angular unconformity.

Along with the continuous weak extension background and extensive transgression, the sedimentary range gradually expanded, and the sediments influenced the filling up and leveling (Zhou et al., 2012). Therefore, most isolated rifts developed in the early–middle Cryogenian were filled with sediments and became gradually connected (Xu et al., 2013a) (Figs. 9 and 10-b). The Tarim Block ended the rifting stage and entered the wide and gentle depression stage when the igneous rock activities were much smaller in scale, and no deep and large rifts appeared. The Tarim Block experienced overall subsidence in this period, where the deposits were small in thickness and large in coverage, and extensive and continuous large shallow-water depressions formed, with fluvial-lacustrine-littoral-shallow marine facies developed around. Sedimentation in the NTT gradually connected into one piece, and ancient land remained only in the north.

Under this tectono-sedimentary background, the global Sturtian and Marinoan glaciations affected wide ranges of the Tarim Block. Glacial marine facies clastic sediments were widely developed, and many marine glaciers floated in the ocean, as confirmed by massive morainic

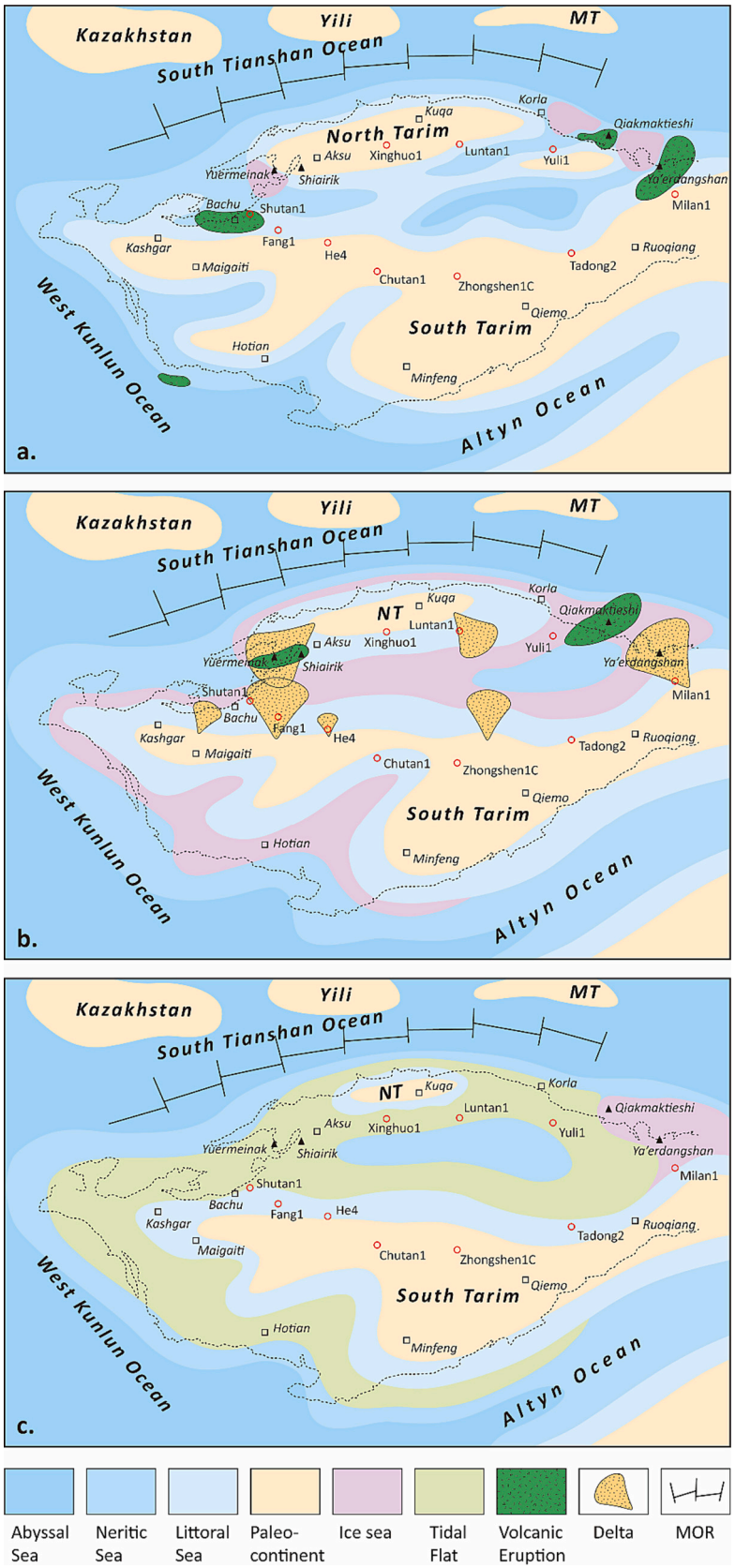

Fig. 10. Paleogeographic evolution in the Tarim Block from the early Cryogenian (a) to late Cryogenian - early Ediacaran (b) and to early Cambrian (c). Note: CT, Central Tianshan; NT, North Tarim; MOR, Mid-ocean ridge.

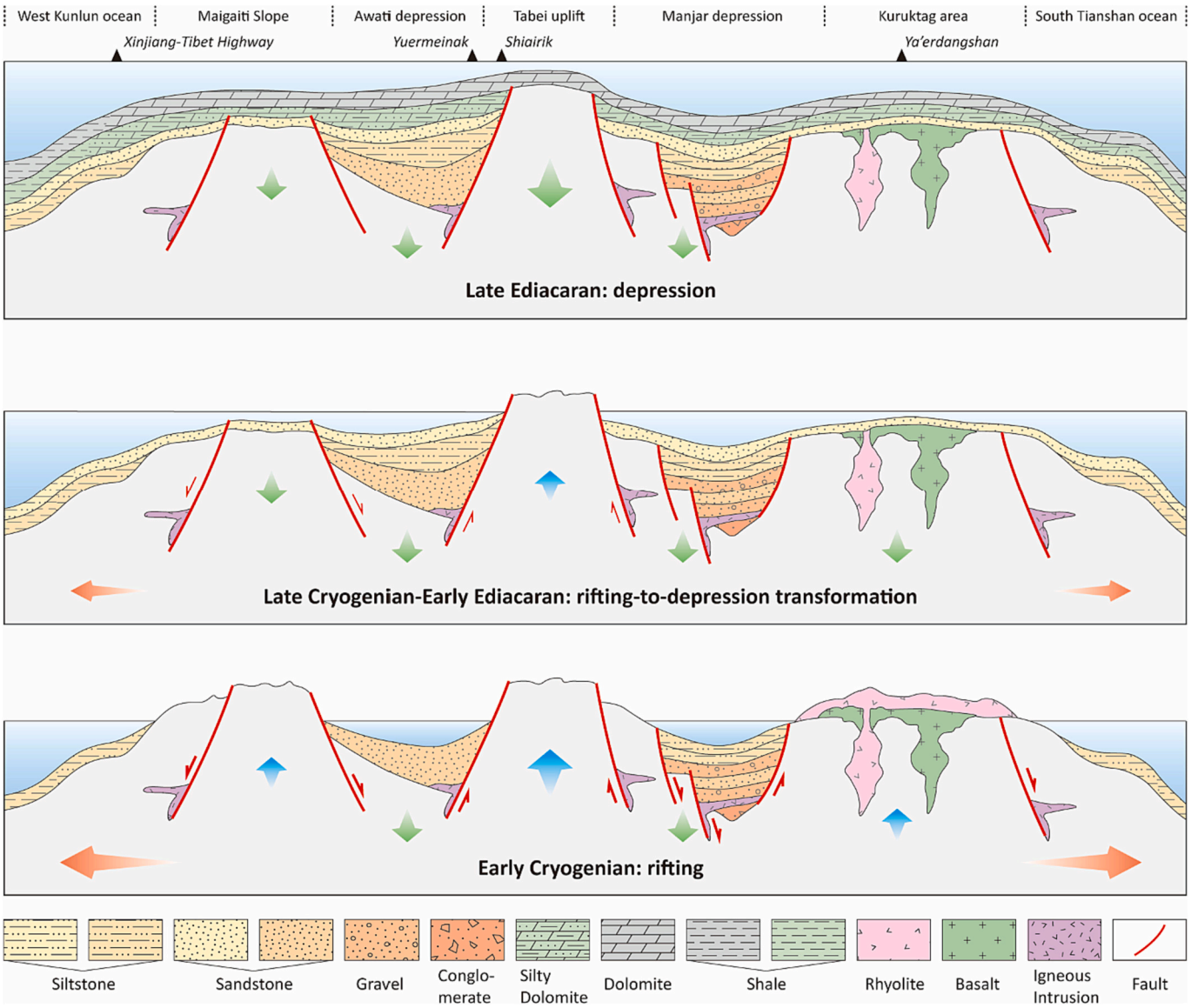

Fig. 11. Tectonic-sedimentary evolution profile in the Tarim Block during Cryogenian to early Cambrian.

conglomerates and diamictites in the field sections around the block (Fig. 3). The diamictites can account for 30% ~ 70% of the total strata in several field sections in the northwest and northeast Tarim Block. Comparingly, the diamictites have a relatively smaller thickness in the Ya'erdangshan area, probably due to the residual heat flow of the Early Cryogenian volcanic rocks (Wu et al., 2017). After each glacial period, the rapid melting of glaciers during the interglacial period rapidly increased the sea level and stronger weathering of the denudation area. In some areas, tidal delta facies of land–sea transition facies were formed, for example, near the rift valleys in Ya'erdangshan and Aksu (Fig. 10-b). The lower part is prodelta facies composed of dark siliceous mudstone with thin layers of quartz siltstone, and the higher part is deltaic front facies containing lithic fine sandstone with thin layers of dolomite. Under the background of large-scale transgression, dark shale stable in distribution was likely to develop in the deep-water area. Simultaneously, as strong upwelling currents and surface runoff with more nutrients promoted the productivity boom, the shale formed in this period is frequently a potential source rock, rich in organic matter.

During the early Ediacaran, most accommodation space of the rift basins were filled, and the Tarim Block has entered the depression stage. Deltaic plain facies with upward coursing sequence were formed due to the increasing clastic provenance in the northeast Ya'erdangshan area. Tidal delta facies were widely formed in both the north and south sides of the rift basin in the Aksu area. Various types of sedimentary structures including herringbone cross-bedding and ripple mark were identified.

5.3. *Late Ediacaran–Early Cambrian*

The Tarim Block was stable in tectonics from the late Ediacaran to the early Cambrian. Unlike in the Cryogenian when rifting dominated, the Tarim Block had a stable tectono-sedimentary system of intracratonic depression established in the late Ediacaran. Most of the rift basins were totally filled in the late Ediacaran. With the weakening of continental breakup and strengthening of transgression, the ancient land in the NTT became smaller, and the primary sedimentary environment in Tarim evolved from a littoral-shallow sea to a more extensive and stable carbonate platform and tidal flat, e.g., the thick carbonates with thin interlayers of mudstone, siltstone, and sandstone in the Shuiquan and Hangelchaok formations. The rocks deposited changed accordingly from clastic to carbonate, and a set of thick-bedded and stably distributed microbial and grain beach dolomite assemblages was deposited, which can be correlated in the peripheral outcrop strata. Tillite also

developed but in a very small range, and continuous tillite deposits formed only in the northeast of the basin (Fig. 10).

At the end of the Ediacaran, the Kalpin movement uplifted most of the Tarim Block and different degrees of denudation of the dolomite member at the top of the Ediacaran. In the NTT, tectonic activities were weak, and thus, a regional parallel unconformity was formed between the Ediacaran and the overlying Cambrian. However, an overlapping-type angular unconformity is observed on the northern flank of the STT uplift belt, indicating that it underwent a sustained and slow uplifting at the end of the Ediacaran. The Tarim Block inherited the tectono-sedimentary framework of the Cryogenian–Ediacaran in the early Cambrian (Pan et al., 2015; Du and Pan, 2016; Guan et al., 2019) and still had the north–south differentiation characteristic of a sedimentary basin. The NTT had a near E–W-trending back-arc rift, where a near E–W-trending deep-water continental shelf developed. On the south and north sides were two paleo-uplifts: Tazhong and Tabei, respectively. Due to the transgression across the Tarim Block in the early Cambrian, an extensive epicontinental shallow sea was formed, and widely distributed Yuertusi Formation shale was deposited (Yan et al., 2019). The STT had subsidence and received sediments along the pre-existing Cryogenian structure first. However, the sedimentary strata were limited in distribution, and the compression and uplift from the southwest margin led to a restricted platform and tidal-flat facies.

6. Formation of petroleum resources in response to tectono-environmental evolution

The Tarim Basin is one of the basins with the most remarkable achievements in ultra-deep oil and gas exploration globally. In particular, several large oil and gas fields have been discovered recently in Cambrian–Ordovician strata with depths of >8000 m, and natural gas pools were discovered in the Ediacaran, attracting the attention of global oil and gas exploration and academic scholars (Yang et al., 2020; Zhu et al., 2021c, 2023a). The Cambrian Yuertusi Formation shale is the major source rock in the basin, and the Cryogenian–Ediacaran has potentially favorable source rocks (Zhu et al., 2018, 2020c, 2022b, 2023b). Due to the huge burial depth (>8000 m), Cryogenian–Cambrian source rocks have not been encountered directly by drillings. However, multiple Cryogenian–Cambrian potential source rocks have been discovered using field surveys, evaluating outcrop samples, and tracking and comparing seismic datasets in the basin. The tectono-environmental evolution in the Tarim Block primarily controls their formation, and the ultra-deep strata have huge potential for petroleum resources.

6.1. Field outcrop characteristics of Cryogenian–Cambrian petroleum source rock

Thick Cryogenian mudstones formed in deep-water facies have been found in four outcrop sections at the margin of the Tarim Block: Aksu Yuermeinak in the northwest, the Xinjiang–Tibet Highway in the southwest, and the north (Qiakmaktieshi) and south (Ya'erdangshan) Kuruktag in the northeast of Tarim (Figs. 1, 12).

In the Qiakmaktieshi section, north Kuruktag area, gray-green and black Tereeken mudstone that formed in basinal facies has the maximum TOC of 0.3%, and Altungal mudstone has a TOC of 0.1%–0.51%, both meeting the standard of poor–medium source rock. On the Ya'erdangshan section in the south Kuruktag area, dark gray-black Tereeken open continental shelf facies muddy shale has a large thickness (>300 m) and high TOC of 0.2%–1.4%. The black, muddy shale in the lower member of the Tereeken Formation has a TOC >0.5%, both meeting the standard of petroleum source rock.

However, the Cryogenian source rock outcrops in the northwest and southwest Tarim are typically severely weathered, making it challenging to obtain fresh samples. The dark gray mudstone unit in the Xifangshan Formation from the Yuermeinak section is approximately 50 m thick; however, this unit is of poor quality, as the TOC is lower than 0.1%. The

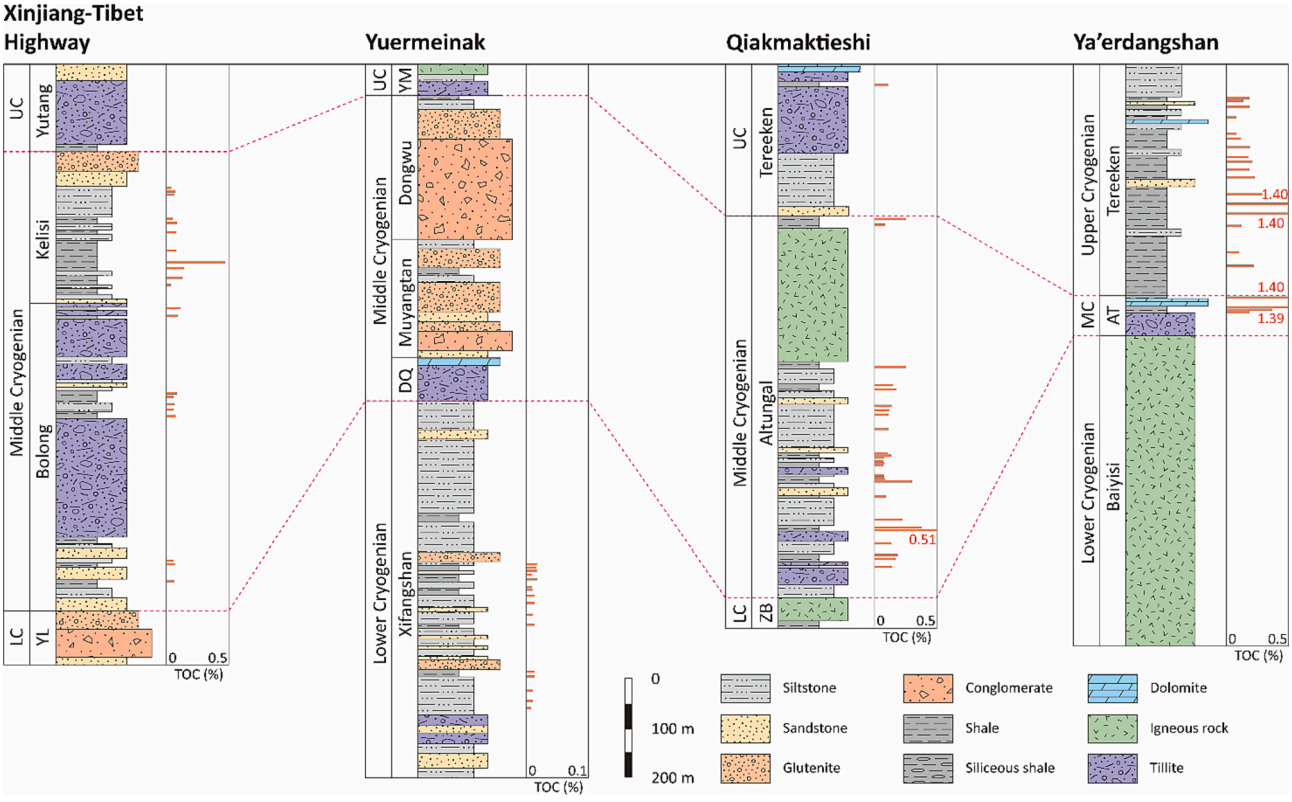

Fig. 12. Lithological characteristics and total carbon content (TOC) of the Cryogenian intervals in outcrops in the Tarim Block (part of the data from Zhu et al., 2020a, 2020c). Note: AT, Altungal; DQ, Dongqiao'enbrak; LC, lower Cryogenian; UC, upper Cryogenian; YL, Yalaguzi; YM, Yuermeinak; ZB, Zhaobishan.

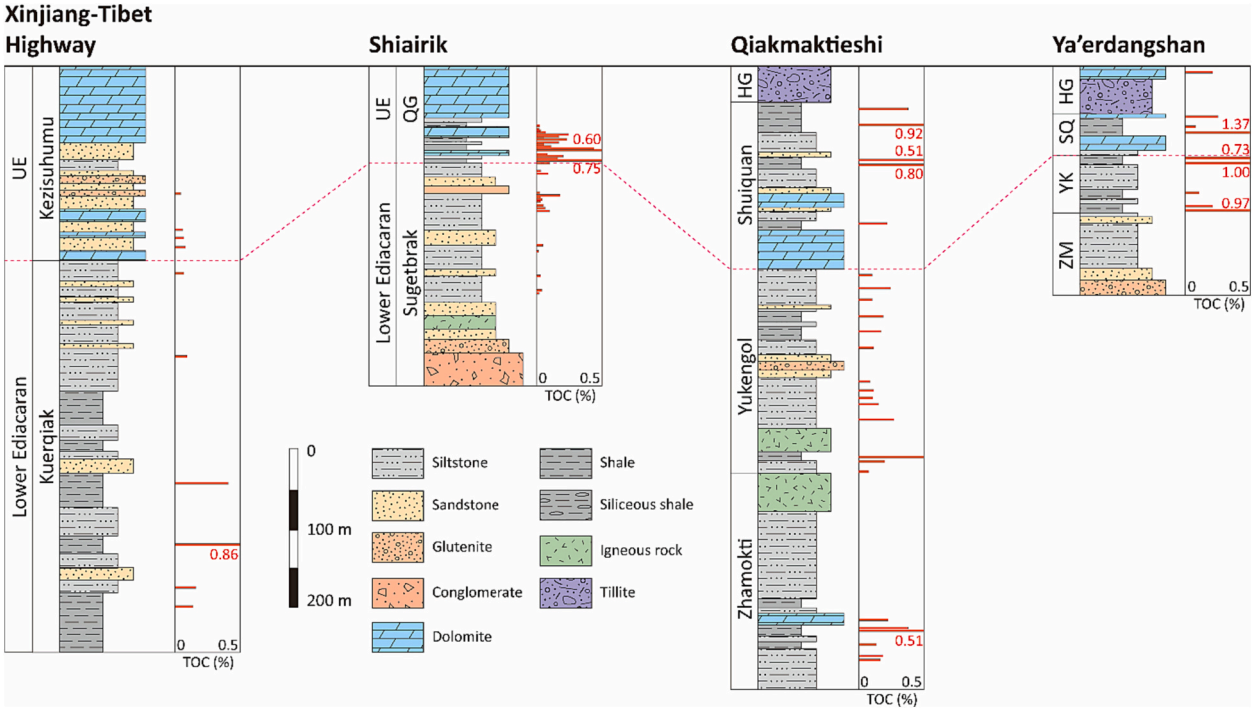

Fig. 13. Lithological characteristics and total carbon content (TOC) of the Ediacaran intervals in outcrops in the Tarim Block (part of the data from Zhu et al., 2020a, 2022a; Zhang et al., 2022). Note: HG: Hangelchaok; QG, Qigbrak; SQ, Shuiquan; UE, upper Ediacaran; YK, Yukengol; ZM, Zhamokti.

thick and silty mudstones in the Kelisi Formation from the Xinjiang–Tibet Highway are >300 m thick and have a low TOC of 0.1%–0.46%.

Unlike the Cryogenian, the Ediacaran typically has thicker mudstone units, considerably varying in different layers and areas (Fig. 13). For the Qiakmaktieshi section in north Kuruktag, the Zhamokti mudstone with a low TOC of 0.1%–0.4% represents nonsource rock. The TOC of Yukengol dark gray, gray, and grayish-black mudstone is 0.2%–0.78%, whereas that of the Shuiquan dark gray and black muddy shale unit with 100 m thickness ranges from 0.2% to 0.92%, representing better quality. On the Ya'erdangshan section in south Kuruktag, the gray-grayish-black silty mudstone unit at the bottom of the Yukengol Formation has a TOC of 0.1%–0.97% and a thickness of 32 m. The dark gray and black shale of the Shuiquan Formation has a TOC of 0.2%–1.37% and a thickness of 40

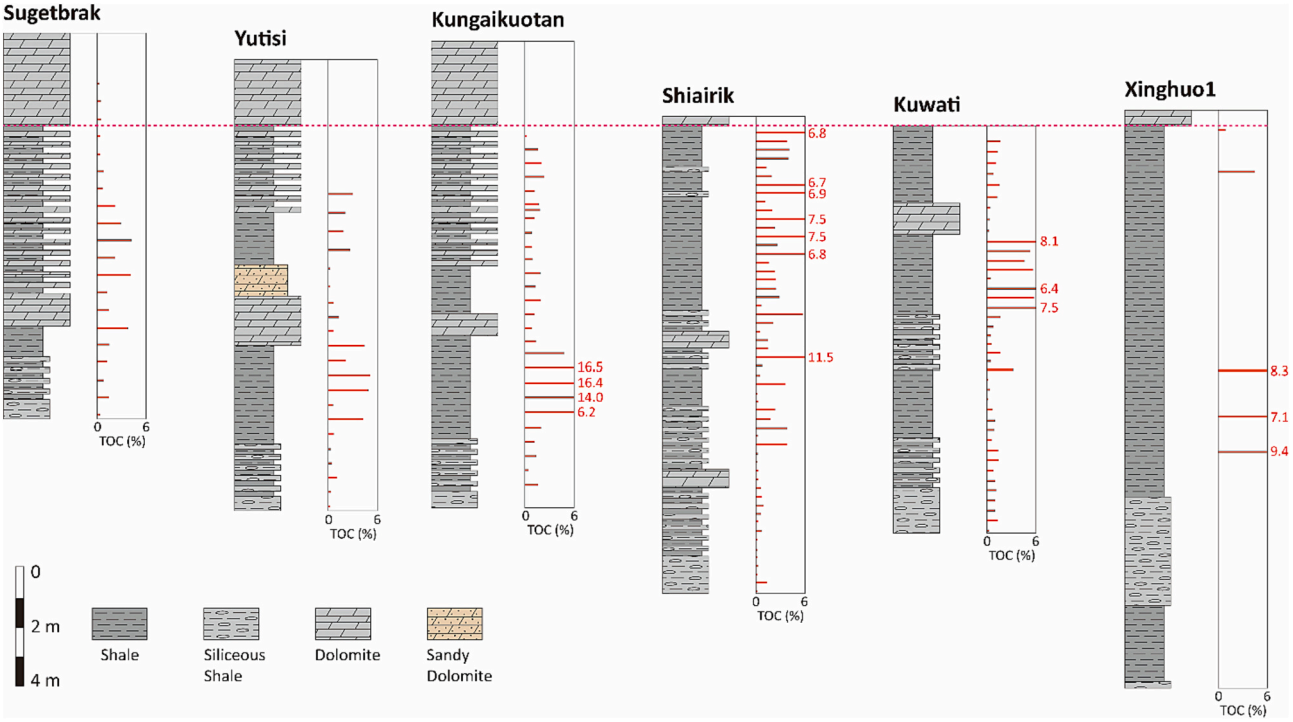

Fig. 14. Lithological characteristics and total carbon content (TOC) of the Cambrian intervals in outcrops in the Tarim Block (part of the data from Zhu et al., 2018, 2020b).

m.

In Aksu, a set of stably distributed dark gray mudstone in the upper part of the Sugetbrak Formation from the Shiairik section has a TOC between 0.2% and 0.75%, of which dark gray mudstone with TOC > 0.5% is approximately 50 m thick, making it the best source rock in the Ediacaran outcrops so far. Thin layers of mudstone in the lower part of the Qigbrak Formation (primarily comprising gray medium-thick layered dolomite) have a TOC of 0.2%–0.5% and can only be classified as a poor source rock.

On the Xinjiang–Tibet Highway section, the grayish-black thin-bedded argillaceous siltstone and mudstone succession of the Kuerkak Formation is approximately 200 m thick, with the highest TOC of 0.86%. The littoral facies grayish-green silty mudstone in the lower member of the Yutang Formation has a TOC of <0.2%, and the silty mudstone in the lower part of the Kezisuhumu Formation has a very low TOC (<0.2%), both failing to meet the standard of petroleum source rock.

The Lower Cambrian source rock outcrops are primarily found in the Aksu area at the northwest margin, and a few wells at the basin margin have encountered thin Lower Cambrian source rocks. Field observations show that the Lower Cambrian strata at different section sites are comparable in lithology, typically comprising grayish-black thin siliceous rock beds at the bottom, black shale in the middle, and gray dolomitic limestone with a small amount of thin dark gray mudstone interbeds at the top (Fig. 14). Abundant phosphatic nodules were observed in the lower part of all section sites. They were formed in a deep-water slope environment. The black shale in the middle member of each section is thick and high in organic matter abundance, indicating undercompensated deep-water basin deposits developed in the middle–lower gentle slope facies belt controlled by upwelling currents. Xinghuo1, a newly drilled well in the basin, encountered a 30 m thick source rock in the Yuertusi Formation. Cuttings analysis shows that this source rock has a TOC of 1.7%–9.4% (Feng et al., 2015). Most of the Lower Cambrian black shale samples from the field outcrops have a TOC of 2%–6%, whereas the samples from the middle part have a higher TOC, up to 17.9% (Zhu et al., 2016), the highest TOC recorded in marine source rocks in the Tarim Basin so far.

6.2. *Formation environments, models, and distribution of the Cryogenian–Cambrian source rocks*

6.2.1. *Cryogenian interglacial rifting-type source rock*

The Tereeken mudstone units in the Ya'erdangshan section are the best quality source rock found in the Cryogenian outcrops of the Tarim Block. Sedimentary sequences, ages of igneous rocks, carbon isotopes, and CIA data confirm that this is a typical interglacial source rock (Zhu et al., 2019, 2020b; Ren et al., 2020) that developed between two glacial periods at 655–635 Ma and represents deep-water deposits in the rift trough during the breakup of continents (He et al., 2014). Its development process can be divided into three stages (Fig. 15).

Stage 1: Following the breakup of the Rodinia supercontinent,

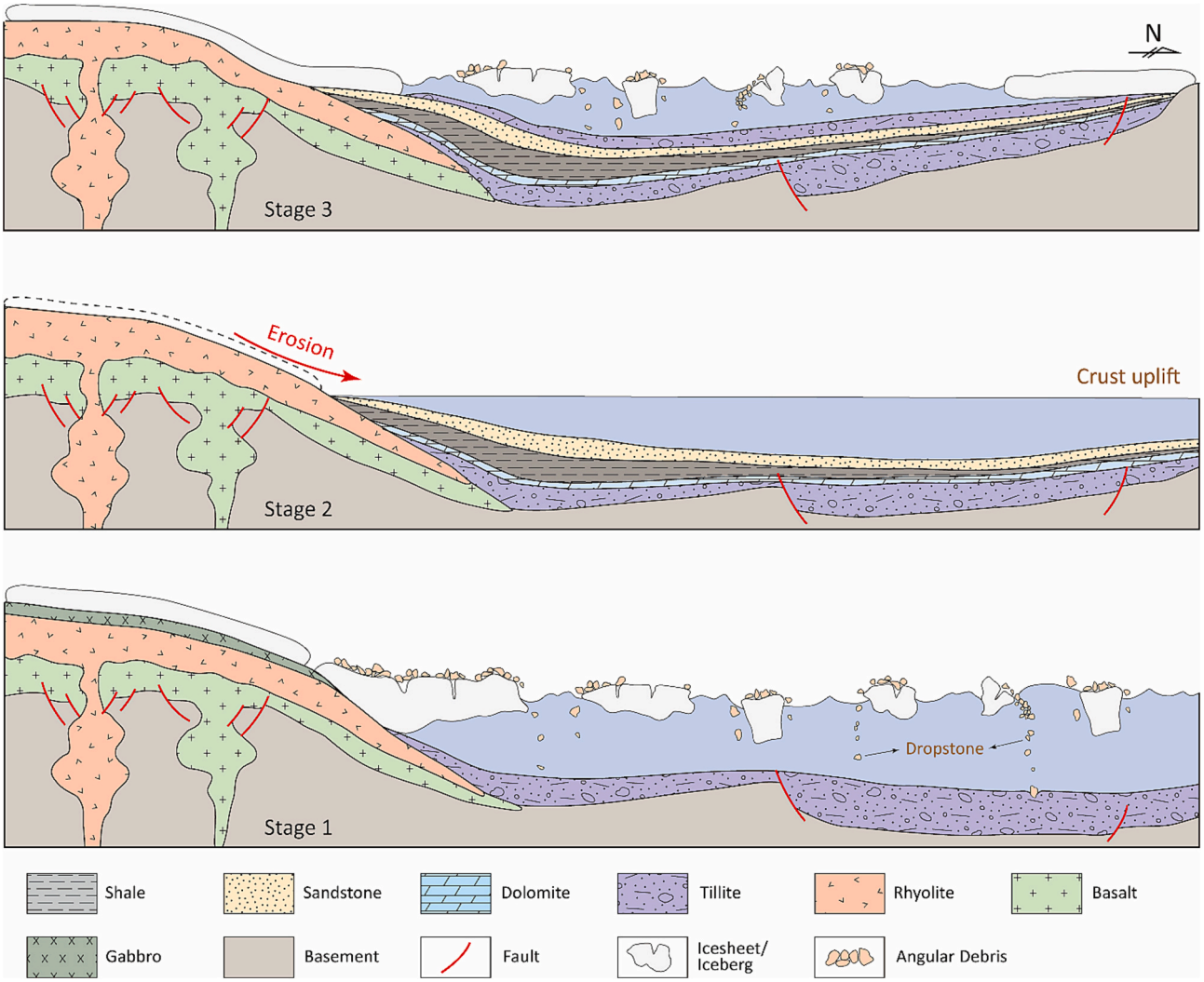

Fig. 15. Cartoon illustrating the formation model of the Cryogenian "interglacial rifting-type" source rock in the Kuruktag area, northeast Tarim Block.

continental rifts developed in the Tarim Block. Due to frequent bimodal volcanic activities in the late Cryogenian, the Kuruktag area evolved into a rift basin with a topography higher in the south and lower in the north. When the second Cryogenian glaciation started, known as the Sturtian, the Kuruktag area was extensively covered by ice sheets. Glacial marine facies in the rift primarily comprise mélange with tillite characteristics. The southern part of the rift records a complete volcanic–clastic sedimentary sequence, whereas the northern part has only a few volcanic rocks preserved. Due to the continuous activities of the southern volcanic center, the CO_2 concentration in the atmosphere increased, and thus, the greenhouse effect increased, and the climate changed from cold to warm. Subsequently, the ice sheets melted, and thin-bedded siliceous and cap dolomites were formed.

Stage 2: With the end of the glacial period, the sea level rose rapidly, and the water body in the Kuruktag area became deeper for a long time. Due to the rapid rifting and drastic change in the water depth, the center of the rift valley turned into a hungry basin. The intensified weathering of peripheral rocks provided sufficient nutrient elements. Thus, marine plankton, prokaryotes (bacteria and blue-green algae), and fungi began to bloom, constituting the material basis of Cryogenian source rocks and promoting the formation of deep-water dark organic-rich shale overlying the cap dolomite in the rift. Later, the Pan-African movement uplifted the entire Kuruktag area (Eyles and Januszczak, 2004; Scheller et al., 2018). The water body became shallower after the large-scale regression, and the sedimentary environment gradually became more oxidized. Accordingly, the rocks deposited transitioned to argillaceous

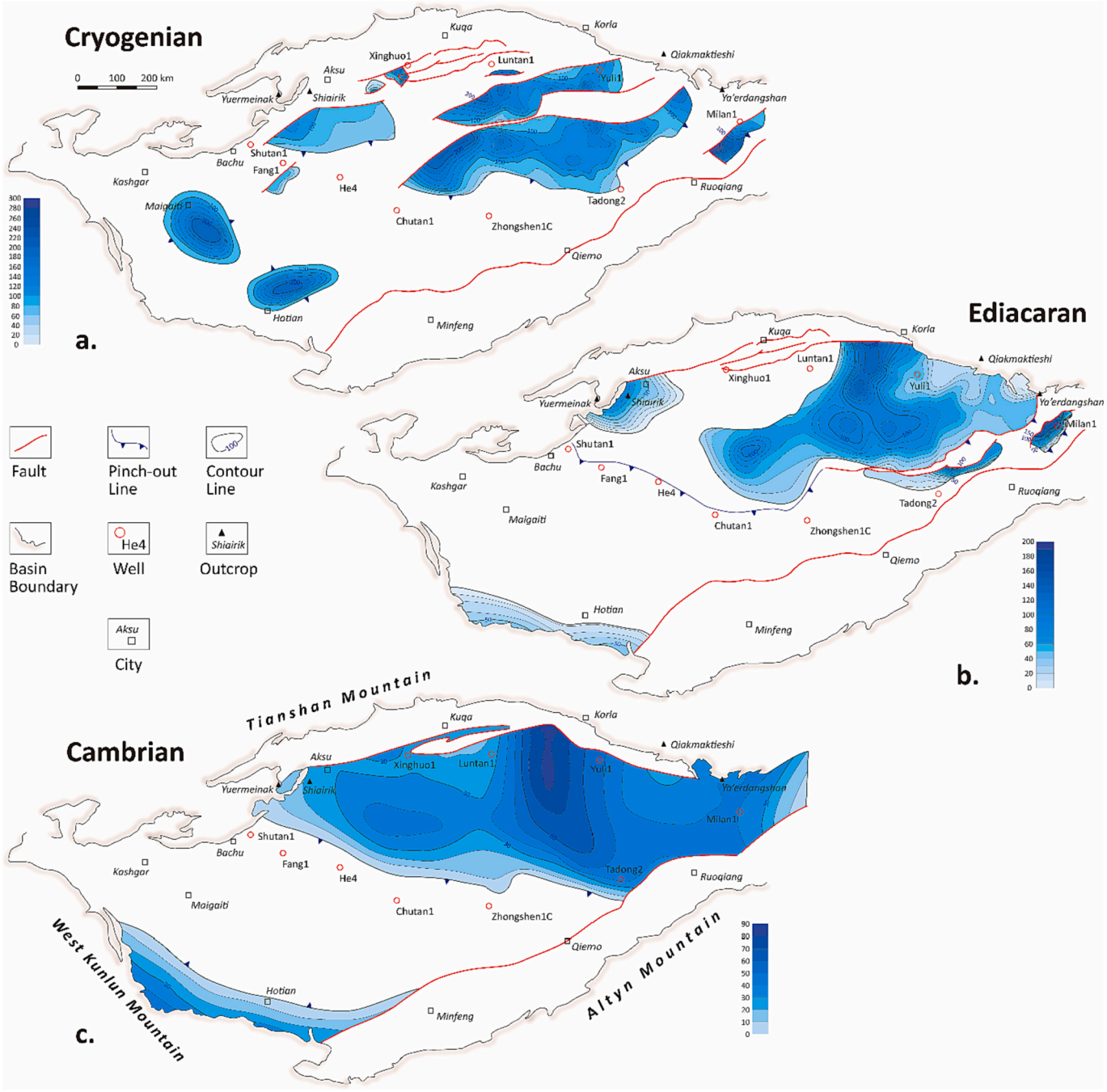

Fig. 16. Estimated distribution and thickness of the Cryogenian, Ediacaran and Cambrian source rocks in the Tarim Block (after Zhu et al., 2018, 2020b; Yan et al., 2019, 2022).

siltstone–sandstone in an oxidation environment.

Stage 3: With the onset of the Marinoan glaciation, the deposition of the clastic rock sequence in the oxidizing environment peaked and was replaced by a suite of tillites. The complex and diverse tillites in the north recorded characteristics of the ice-rafting deposits during the glacial period and the mixed normal shallow marine and glacial water deposits during the glacial melting period. In the southern part, as the mantle magma increased the crustal heat flow values, the tillites became thinner and pinched out to higher positions. Deposits in this period primarily comprise silty mudstone, sandstone, and crystal powder dolomite at local positions, with granularity coarsening from the bottom to the top. The global climate gradually warmed, and a new round of mudstone was deposited.

The rift system primarily controls the distribution of the Cryogenian source rocks, as evidenced by the thickness of outcrop intervals, development environments and sedimentary characteristics of the source rocks, and seismic reflection characteristics in the basin (Fig. 16-a). Several NE-trending single-fault or double-fault rifts occur in the northern part of the basin, each with a corresponding depocenter. The source rock in a rift is thickest at the center of the rift valley or on the fault side of the single-fault rift. Cryogenian source rocks are the thickest in the northeast of the basin, whereas they only occur in a limited scope in the west.

6.2.2. *Ediacaran weak extensional depression-type source rock*

Mudstone units from the Sugetbrak Formation in Aksu are potential petroleum source rocks with stable distribution. They were formed in a large shallow-water depression under a weak extensional background after completing the rift-depression transformation in the Tarim Block. According to the tectono-sedimentary evolution in Aksu, the formation of Sugetbrak source rocks can be divided into two stages (Fig. 17).

Stage 1 is the development period of the continental arc basin related to subduction at the northwestern margin of the Tarim Block. The blueschist metamorphism and the long-time arc-affinity igneous activities (900–740 Ma) of the Aksu Group indicate that subduction–collision orogenic tectonic settings dominated the Aksu area (Zhu et al., 2011). The subduction lasted until 760 Ma, giving rise to many mafic dyke swarms with arc-like characteristics. In this period, the intracontinental rifts were close to the provenances, and the sedimentary fillings were primarily a small fan-delta-fluvial–lacustrine sedimentary system. With the filling up and leveling of sediments, most isolated preexisting rifts were filled and gradually became connected, facilitating the end of the rifting stage of the northern Tarim.

Stage 2 represents the transition from subduction to weak extensional settings in the northern Tarim. The CFB at the bottom of the Sugetbrak Formation has similar geochemical characteristics with the standard OIB, indicating that the Sugetbrak basalt formed in an intracontinental rift environment, and its formation is related to the partial melting of the lithospheric mantle caused by the upwelling of the asthenospheric mantle (Zhang et al., 2012a, B; Xu et al., 2013a, 2013b; Chen et al., 2020; Zhu et al., 2022a). At this stage, Aksu, with igneous activities much smaller in scale, was in an overall weak extensional tectonic background. The area entered a wide and gentle depression stage and experienced subsidence under continuous transgression. Large-scale depressions dominated the sedimentary environment, and the strong upwelling currents and surface runoff promoted the eutrophication of the water body and the booming of productivity; therefore, dark shale was likely to develop in the deeper slope-shelf facies. Although with a small thickness, the dark shale has a large coverage and stable distribution and can be classified as a potential source rock, rich in organic matter.

On seismic sections, the Ediacaran appears as depression deposits controlled by Cryogenian rifts. It comprises large deposits in broad and gentle accommodation spaces over large scopes (Fig. 16-b). The

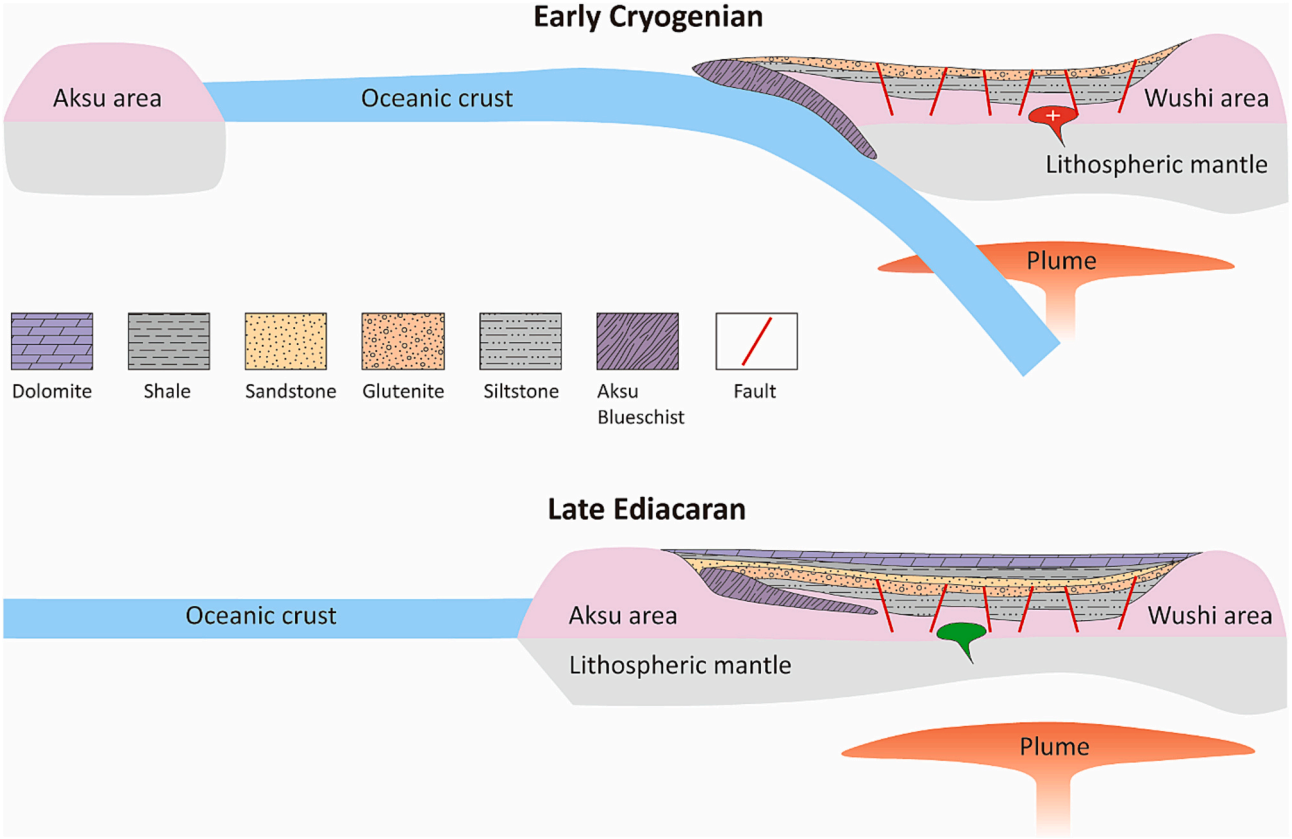

Fig. 17. Cartoon illustrating the formation model of the Ediacaran "weak extensional depression-type" source rock in the Aksu area, northwest Tarim Block.

Ediacaran source rocks have multiple depocenters: the northern depocenter is northwest of the Manjar Depression, where the source rocks are approximately 300 m thick. In eastern Tarim, as affected by the rifts in the south, the bottom of the Ediacaran could have the formation conditions for petroleum source rock, but it might be thinner. Regarding the slope zone in the northwest and the piedmont zone in the southwest of Tarim, as affected by the Ediacaran paleogeomorphology, gentle slope source rocks are readily formed with a limited range.

6.2.3. Cambrian transgression-induced gentle slope-type source rock

During the early Cambrian, the Tarim Block inherited the Ediacaran tectonic framework and had an extensive epicontinental shallow sea developed under global transgression. An anoxic sulfide environment favorable for organic matter preservation was formed in the middle-to-lower gentle slopes (Fig. 18). Hydrothermal activities and coastal upwelling currents brought more metal elements and nutrients into the water body, causing the blooming of phytoplankton and benthic algae in the coastal area (Zhu et al., 2018; Sun et al., 2022). Consequently, biological yield and water productivity soared and became a significant organic matter source. The dissolved oxygen in the seawater was consumed during the organic matter sedimentation, leading to the gradual upward movement of the oxygen minimum zone. Reducing gases (primarily H_2S) brought by the hydrothermal fluid further aggravated the anoxic degree of the bottom water body, attributing to favorable conditions for the burial and preservation of vast organic matter, and finally, formed this set of organic-rich source rock.

The Yuertusi source rock has the best quality ever discovered in the Tarim Basin, with a stabler thickness in the platform–basinal areas than those of the Cryogenian–Ediacaran. The strong seismic reflection characteristics of the Cambrian bottom boundary are steady, easily identified, and can be traced across the entire basin (Fig. 16-c). This set of source rocks has three depocenters, and the east and west Manjar sags are the main ones, with a thickness up to >100 m. The Yuertusi source rock in the southwest of Tarim might occur limited in strips, are thin, and pinch out to the north. Combined with the overlying high-quality thick dolomite reservoir in the Xiao'erbrak Formation and the favorable caprock in the middle Cambrian, they constitute the best accumulation assemblage in the ultra-deep layers in the Tarim Basin. With the industrial discoveries achieved in wells ZS1C and LT1, this accumulation assemblage is the most realistic ultra-deep exploration zone with huge resource potential in the basin.

7. Conclusions

The Tarim Block has experienced complex tectono-sedimentary evolution during the transition from the Rodinia breakup to the Gondwana supercontinent assemblage, as evidenced by the various sedimentary sequences and multiphase igneous activities. This study has provided a synthesis of the well-preserved Cryogenian–Cambrian sequences in the Tarim Block, and the primary conclusions are as follows.

(1) The Tarim Block comprises two discrete terranes, SST and NTT, as they differ significantly in the characteristics of Precambrian basements, geodynamic background, and rift formation mechanisms due to the geochemistry of the five phases of igneous records during the Cryogenian to the Cambrian and the position of Tarim in the Rodinia supercontinent. Cryogenian rifts in the STT were formed due to the upwelling of the Rodinia super-mantle plume, whereas those in the NTT were primarily attributed to the back-arc extension by the Circum–Rodinia subduction rather than the plume. With the gradual weakening of subduction during the Ediacaran, the plume primarily affected the STT and NTT. However, due to the weak extensional background, the Tarim Block entered the depression stage and evolved into a passive continental margin environment in the late Ediacaran and early Cambrian.

(2) Four sets of Neoproterozoic tillites and five sets of volcanic rocks crop out in the Kuruktag area of northeast Tarim, providing an excellent example for studying glacial–interglacial evolution. As constrained by age data from igneous rocks or detrital zircons, these four glaciers correlate globally with the Kaigas, Marinoan, Sturtian, and Gaskier glacial events. Sedimentary sequences and geochemical characteristics revealed the paleoclimate and environmental changes during the glacial–interglacial cycles. Generally, intensive silicate weathering caused the increasing consumption of CO_2, strengthening the ice house effect and forming thick tillites with typical glacial marks. Due to volcanic eruptions during the glacial period, many greenhouse gases were released. Elevated temperatures, humidity, and sea levels intensified the continental weathering, bringing nutrients into the seawater and promoting the bloom of early life and recovery of paleoproductivity in the ocean.

(3) The tectonic evolution controlled the sedimentary environment and sequences. Rifting in STT and NTT was intensive due to the super-mantle plume or subduction zone during the Cryogenian; thus, the rifts were isolated and limitedly distributed but with thick deep-sea rift

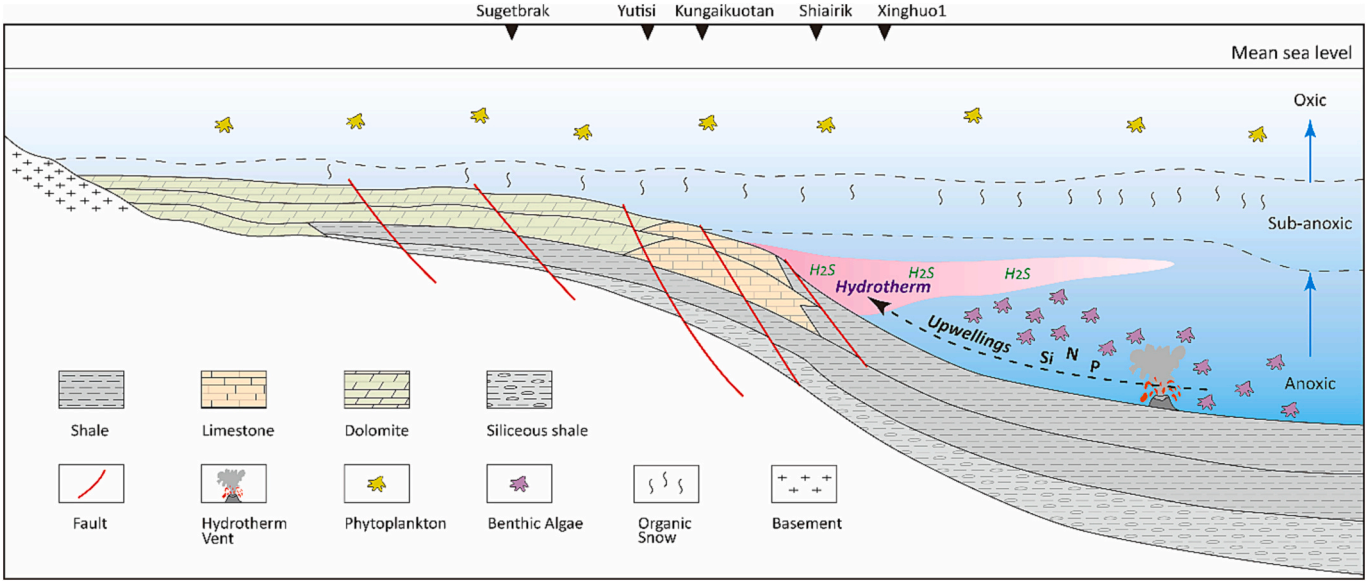

Fig. 18. Cartoon illustrating the formation model of the Cambrian "transgression induced gentle slope-type" source rock in the Aksu area, northwest Tarim Block. Note: H_2S, Hydrogen Sulfide.

deposits. As the extensional tectonic settings weakened and transgression intensified during the early Ediacaran, the sedimentary range gradually expanded with filling up and leveling features. Most isolated rifts were thus filled and connected. In the early Cambrian, the Tarim Block was stable in tectonics, and the primary sedimentary environment in Tarim evolved from a littoral-shallow sea to a more extensive and stable carbonate platform and tidal flat.

(4) Interglacial mudstone units can form effective petroleum source rocks, e.g., the lower Tereeken black shale (TOC > 0.5%) and Shuiquan dark gray-black muddy shale (TOC up to 1.37%) in Kuruktag, the upper Sugetbrak dark gray mudstone (50 m in total with TOC > 0.5%) in Aksu, and the Kuerkak grayish-black mudstone (TOC up to 0.8%) in Tieklik. According to the tectonic evolution process, three formation models of favorable petroleum source rock were proposed as the Cryogenian interglacial rifting type, the Ediacaran weak extensional depression type, and the Cambrian transgression-induced gentle slope type. The distribution of each source rock was estimated accordingly. It further indicates that great potential for oil/gas resources remains in ancient Cryogenian–Cambrian assemblages, despite their huge burial depth within the Tarim Basin.

Declaration of Competing Interest

The authors declare that they have no known competing financial interests or personal relationships that could have appeared to influence the work reported in this paper.

Data availability

Data will be made available on request.

Acknowledgements

The Tarim Oilfield, PetroChina is acknowledged for contribution in sampling, seismic data and field basic data collection. We acknowledge the editor Dr. Yildirim Dilek, guest editor Prof. Ian Somerville and two anonymous reviewers for their constructive suggestions that substantially improved the quality of this manuscript. We thank the Key Laboratory of Petroleum Geology at the Research Institute of Petroleum Exploration and Development, PetroChina, and the Key Laboratory of Tectonic and Petroleum Resources at China University of Geosciences for help with geochemical analysis. This work was financially supported by National Natural Science Foundation of China (Grant Nos. 42002178, 42230812) and Scientific Research and Technology Development Project from China National Petroleum Corporation (Grant No. 2021DJ05).

References

Allen, P.A., Etienne, J.L., 2008. Sedimentary challenge to Snowball Earth. Nat. Geosci. 1, 817–825.
Bowring, S., Myrow, P., Landing, E., Ramezani, J., Grotzinger, J., 2003. Geochronological constraints on terminal Neoproterozoic events and the rise of metazoans. Geophys. Res. Abstr. 5, 13219.
Brasier, M., McCarron, G., Tucker, R., Leather, J., Allen, P., Shields, G., 2000. New U-Pb zircon dates for the Neoproterozoic Ghubrah glaciation and for the top of the Huqf Supergroup, Oman. Geology 28, 175–178.
Cai, Z., He, B., Meert, J.G., Ma, X., Jiao, C., Liu, R., Chen, X., Yun, X., 2021. Neoproterozoic tectonic transition from subduction-related convergence to continental extension of the Tarim Block, NW China. Precambrian Res. 362, 106278.
Chen, Y., Xu, B., Zhan, S., Li, Y., 2004. First mid-Neoproterozoic paleomagnetic results from the Tarim Basin (NW China) and their geodynamic implications. Precambrian Res. 133, 271–281.
Chen, W., Zhu, G., Zhang, K., Zhang, Y., Yan, H., Du, D., Zhang, Z., Xia, B., 2020. Late Neoproterozoic intracontinental rifting of the Tarim carton, NW China: an integrated geochemical, geochronological and Sr–Nd–Hf isotopic study of siliciclastic rocks and basalts from deep drilling cores. Gondwana Res. 80, 142–156.
Craig, J., Thurow, J., Thusu, B., Whitham, A., Abutarruma, Y., 2009. Global Neoproterozoic petroleum systems and the emerging potential in North Africa. In: Craig, J., Thurow, J., Whitham, A., Abutarruma, Y. (Eds.), Global Neoproterozoic Petroleum Systems: The Emerging Potential in North Africa. Geological Society. Special Publication, London, pp. 1–24.
Craig, J., Bif, U., Galimberti, R.F., Ghori, K.A.R., Gorter, J.D., Hakhoo, N., Le Heron, D.P., Thurow, J., Vecoli, M., 2013. The palaeobiology and geochemistry of Precambrian hydrocarbon source rocks. Mar. Pet. Geol. 40, 1–47.
Cui, H., Tian, L., Zhang, N., Liu, J., 2016. Nanhua-Sinian rift distribution and its relationship with the development of Lower Cambrian source rocks in the southwest depression of Tarim Basin. Acta Pet. Sin. 37 (4), 430–438.
Deng, X.L., Shu, L.S., Zhu, W.B., 2008. Geochronology of the Precambrian structure-magmatism-deformation along the Xindi fault in Xinjiang, NW China. Acta Petrol. Sin. 24, 2800–2808.
Du, J., Pan, W., 2016. Accumulation conditions and play targets of oil and gas in the Cambrian subsalt dolomite, Tarim Basin, NW China. Pet. Explor. Dev. 43 (3), 327–339.
Eyles, N., Januszczak, N., 2004. Zipper-rift: a tectonic model for Neoproterozoic glaciations during the breakup of Rodinia after 750 Ma. Earth Sci. Rev. 65, 1–73.
Fanning, C.M., Link, P.K., 2004. U-Pb SHRIMP ages of Neoproterozoic (Sturtian) glaciogenic Pocatello Formation, southeastern Idaho. Geology 32, 881–884.
Feng, X., Liu, Y., Han, C., Yan, W., Dong, L., He, Y., 2015. Sinian rift valley development characteristics in Tarim basin and its guidance on hydrocarbon exploration. Petrol. Geol. Eng. 2, 5–10.
Frimmel, H.E., Klötzli, U.S., Siegfried, P.R., 1996. New Pb-Pb single zircon age constraints on the timing of Neoproterozoic glaciation and continental break-up in Namibia. J. Geol. 104, 459–469.
Gao, Z., Cheng, S., 1984. Possible oil-gas-bearing formations in the early Paleozoic and old-age carbonatites of the Tarim Platform. Xinjiang Geol. 2 (1), 1–10.
Gao, L., Guo, X., Ding, X., Zong, W., Gao, Z., Zhang, C., Wang, Z., 2013. Nanhua glaciation event and its stratigraphic correlation in Tarim Plate, China. Acta Geosci. Sin. 34 (1), 39–57.
Ge, R., Zhu, W., Wilde, S.A., He, J., Cui, X., Wang, X., Zheng, B., 2014. Neoproterozoic to Paleozoic long-lived accretionary orogeny in the northern Tarim Craton. Tectonics 33, 302–329.
Giddings, J.A., Wallace, M.W., 2009. Sedimentology and C-isotope geochemistry of the 'Sturtian' cap carbonate, South Australia. Sediment. Geol. 216 (1–2), 1–14.
Guan, S., Wu, L., Ren, R., Zhu, G., Peng, Z., Zhao, W., Li, J., 2017. Distribution and petroleum prospect of Precambrian rifts in the main cratons, China. Acta Pet. Sin. 38, 9–22.
Guan, S., Zhang, C., Ren, R., Zhang, S., Wu, L., Wang, L., Ma, P., Han, C., 2019. Early Cambrian syndepositional structure of the northern Tarim Basin and a discussion of Cambrian subsalt and deep exploration. Pet. Explor. Dev. 46, 1075–1086.
Guo, Z.J., Yin, A., Robinson, A., Jia, C.Z., 2005. Geochronology and geochemistry of deep-drill-core samples from the basement of the central Tarim basin. J. Asian Earth Sci. 25, 45–56.
Halverson, G.P., Hurtgen, M.T., 2007. Ediacaran growth of the marine sulfate reservoir. Earth Planet. Sci. Lett. 263 (1–2), 32–44.
Halverson, G.P., Maloof, A.C., Hoffman, P.F., 2004. The Marinoan glaciation (Neoproterozoic) in Northeast Svalbard. Basin Res. 16 (3), 297–324.
Halverson, G.P., Hoffman, P.F., Schrag, D.P., Maloof, A.C., Rice, A.H.N., 2005. Toward a Neoproterozoic composite carbon-isotope record. GSA Bull. 117, 1181–1207.
Han, J., Wu, G., Xiao, Z., Su, Z., Zhang, L., Li, H., 2020. Recognition of the distribution of Cambrian source rocks and its significance for exploration in Tarim Basin. Chinese J. Geol. 55 (1), 17–29.
He, B.Z., Jiao, C.L., Cai, Z.H., Zhang, M., Gao, A.R., 2011. A new interpretation of the high aeromagnetic anomaly zone in central Tarim Basin. China Geology 38, 961–969.
He, Z.Y., Zhang, Z.M., Zong, K.Q., Dong, X., 2013. Paleoproterozoic crustal evolution of the Tarim Craton: constrained by zircon U–Pb and Hf isotopes of meta-igneous rocks from Korla and Dunhuang. J. Asian Earth Sci. 78, 54–70.
He, J.W., Zhu, W.B., Ge, R.F., 2014. New age constraints on Neoproterozoic diamicites in Kuruktag, NW China and Precambrian crustal evolution of the Tarim Craton. Precambrian Res. 241, 44–60.
He, B., Jiao, C., Huang, T., Zhou, X., Cai, Z., Cao, Z., Jiang, Z., Cui, J., Yu, Z., Chen, W., Liu, R., Yun, X., Hao, G., 2019a. Structural architecture of Neoproterozoic rifting depression groups in the Tarim Basin and their formation dynamics. Sci. China Earth Sci. 62, 529–549.
He, J., Xu, B., Li, D., 2019b. Newly discovered early Neoproterozoic (ca. 900 Ma) andesitic rocks in the northwestern Tarim Craton: implications for the reconstruction of the Rodinia supercontinent. Precambrian Res. 325, 55–68.
He, B., Jiao, C., Liu, R., Cao, Z., Cai, Z., Lan, M., Yun, X., Zhu, D., Jiang, Z., Yang, Y., Li, Z., 2023. The paleotectonic and paleogeography of Neoproterozoic in the Tarim Basin and the prediction of favorable deep source rock areas. Earth Sci. Front. 30 (04), 19-42.
He, J., Pan, X., Li, S., Li, D., Tao, X., Xu, B., 2021. Early Neoproterozoic continuous oceanic subduction along the northern margin of the Tarim Block: insights from ca. 910–870 Ma arc-related magmatism in the Aksu area, NW China. Precambrian Res. 360, 106236.
Hoffman, P.F., Kaufman, A.J., Halverson, G.P., Schrag, D.P., 1998. A Neoproterozoic snowball Earth. Science 281, 1342–1346.
Hoffman, P.F., Halverson, G.P., Grotzinger, J.P., 2002. Are Proterozoic cap carbonates and isotopic excursions a record of gas hydrate destabilization following Earth's coldest intervals?: comment. Geology 30, 286–287.
Hoffman, P.F., Abbot, D.S., Ashkenazy, Y., Benn, D.I., Brocks, J.J., Cohen, P.A., Cox, G. M., Creveling, J.R., Donnadieu, Y., Erwin, D.H., Fairchild, I.J., Ferreira, D., Goodman, J.C., Halverson, G.P., Jansen, M.F., Le Hir, G., Love, G.D., Macdonald, F. A., Maloof, A.C., Partin, C.A., Ramstein, G., Rose, B.E.J., Rose, C.V., Sadler, P.M., Tziperman, E., Voigt, A., Warren, S.G., 2017. Snowball Earth climate dynamics and Cryogenian geology-geobiology. Sci. Adv. 3, e1600983.

Hurtgen, M.T., Arthur, M.A., Suits, N.S., Kaufman, A.J., 2002. The sulfur isotopic composition of Neoproterozoic seawater sulfate: implications for a snowball Earth? Earth Planet. Sci. Lett. 203, 413–429.
Imbrie, J., Boyle, E.A., Clemens, S.C., Duffy, A., Howard, W.R., Kukla, G., Kutzbach, J., Martinson, D.G., McIntyre, A., Mix, A.C., Molfino, B., Morley, J.J., Peterson, L.C., Pisias, N.G., Prell, W.L., Raymo, M.E., Shackleton, N.J., Toggweiler, J.R., 1992. On the structure and origin of major glaciation cycles 1. Linear responses to Milankovitch forcing. Paleoceanogr. Paleoclimatol. 7, 701–738.
Jia, C., 1999. Structural characteristics and oil/gas accumulative regularity in Tarim Basin. Xinjiang Petrol. Geol. 20 (3), 177–183.
Kendall, B., Creaser, R.A., Selby, D., 2006. Re-Os geochronology of postglacial black shales in Australia: constraints on the timing of "Sturtian" glaciation. Geology 34 (9), 729–732.
Kunzmann, M., Halverson, G.P., Scott, C., Minarik, W.G., Wing, B.A., 2015. Geochemistry of Neoproterozoic black shales from Svalbard: implications for oceanic redox conditions spanning Cryogenian glaciations. Chem. Geol. 417, 383–393.
Le Heron, D.P., Cox, G., Trundley, A., Collins, A.S., 2011. Two Cryogenian glacial successions compared: aspects of the Sturt and Elatina sediment records of South Australia. Precambrian Res. 186, 147–168.
Li, H.Q., Xie, C.F., Chang, H.L., Cai, H., Zhu, J.P., Zhou, S., 1998. Study on the Metallogenetic Chronology of Nonferrous and Precious Metallic Ore Deposits in North Xinjiang. Geological Publishing House, China, Beijing, pp. 1–250.
Li, Y.J., Song, W.J., Wu, G.Y., Wang, Y.F., Li, Y.P., Zheng, D.M., 2005a. Jinning granodiorite and diorite deeply concealed in the Central Tarim Basin. Sci. China (D-Series) 48, 2061–2068.
Li, X.H., Su, L., Chung, S.L., Li, Z.X., Liu, Y., Song, B., Liu, D.Y., 2005b. Formation of the Jinchuan ultramafic intrusion and the world's third largest Ni–Cu sulfide deposit: associated with the ~825 Ma south China mantle plume? Geochem. Geophys. Geosyst. 6 (11), Q11004.
Li, Z.X., Bogdanova, S.V., Collins, A.S., Davidson, A., De Waele, B., Ernst, R.E., Fitzsimons, I.C.W., Fuck, R.A., Gladkochub, D.P., Jacobs, J., Karlstrom, K.E., Lu, S., Natapov, L.M., Pease, V., Pisarevsky, S.A., Thrane, K., Vernikovsky, V., 2008. Assembly, configuration, and break-up history of Rodinia: a synthesis. Precambrian Res. 160, 179–210.
Li, X., Li, W., Li, Z., Lo, C., Wang, J., Ye, M., Yang, Y., 2009. Amalgamation between the Yangtze and Cathaysia Blocks in South China: Constraints from SHRIMP U-Pb zircon ages, geochemistry and Nd-Hf isotopes of the Shuangxiwu volcanic rocks. Precambrian Res. 174, 117–128.
Li, Z.X., Evans, D.A.D., Halverson, G.P., 2013. Neoproterozoic glaciations in a revised global palaeogeography from the breakup of Rodinia to the assembly of Gondwanaland. Sediment. Geol. 294, 219–232.
Li, W.S., Li, J.H., Zhou, X.B., Li, W.B., Wang, H.H., Yang, J.Y., 2014. Genesis of high aeromagnetic anomaly zone in Central Tarim Basin: new evidence from seismic profiles. Acta Sci. Nat. Univ. Pekin. 50, 281–287.
Liou, J.G., Graham, S.A., Maruyama, S., Zhang, R.Y., 1996. Characteristics and tectonic significance of the late Proterozoic Aksu blueschists and diabasic dikes northwest Xinjiang, China. Int. Geol. Rev. 38, 228–244.
Liu, Z., Jiang, Y.-H., Jia, R.-Y., Zhao, P., Zhou, Q., 2015. Origin of Late Triassic high-K calc-alkaline granitoids and their potassic microgranular enclaves from the western Tibet Plateau, northwest China: implications for Paleo-Tethys evolution. Gondwana Res. 27 (1), 326–341.
Long, X.P., Yuan, C., Sun, M., Kröner, A., Zhao, G.C., Wilde, S., Hu, A.Q., 2011. Reworking of the Tarim Craton by underplating of mantle plume-derived magmas: evidence from Neoproterozoic granitoids in the Kuluketage area, NW China. Precambrian Res. 187, 1–14.
Long, X.P., Xu, B., Yuan, C., Zhang, C.L., Zhang, L., 2019. Precambrian crustal evolution of the southwestern Tarim Craton, NW China: Constraints from new detrital zircon ages and Hf isotopic data of the Neoproterozoic metasedimentary rocks. Precambrian Res. 334, 105473.
Love, G.D., Grosjean, E., Stalvies, C., Fike, D.A., Grotzinger, J.P., Bradley, A.S., Kelly, A. E., Bhatia, M., Meredith, W., Snape, C.E., Bowring, S.A., Condon, D.J., Summons, R. E., 2009. Fossil steroids record the appearance of Demospongiae during the Cryogenian period. Nature 457, 718–721.
Luo, Z., Xu, B., He, J., 2016. U-Pb detrital zircon age constraints on the Neoproterozoic Tereeken glaciation in the Quruqtagh area, northwestern China. Beijing Daxue Xuebao (Ziran Kexue Ban)/Acta Scientiarum Naturalium Universitatis Pekinensis 52, 467–474.
Macdonald, F.A., Schmitz, M.D., Crowley, J.L., Roots, C.F., Jones, D.S., Maloof, A.C., Strauss, J.V., Cohen, P.A., Johnston, D.T., Schrag, D.P., 2010. Calibrating the Cryogenian. Science 327, 1241–1243.
McLennan, S.M., 1993. Weathering and global denudation. J. Geol. 101 (2), 295–303.
Nesbitt, H.W., Young, G.M., 1982. Early Proterozoic climates and plate motions inferred from major element chemistry of lutites. Nature 299 (5885), 715–717.
Ni, N., Chen, N.H., Ernst, R., Yang, S.F., Chen, J., 2018. Semi-automatic extraction and mapping of dyke swarms based on multiresolution remote sensing images: applied to the dykes in the Kuluketage region in the northeastern Tarim Block. Precambrian Res. 329, 262–272.
Pan, W., Chen, Y., Xiong, Y., Li, B., Xiong, R., 2015. Sedimentary facies research and implications to advantaged exploration regions on lower Cambrian source rocks, Tarim Basin. Nat. Gas Geosci. 26 (7), 1224–1232.
Peng, Y.B., Bao, H.M., Zhou, C.M., Yuan, X.L., 2011. ^{17}O-depleted barite from two Marinoan cap dolostone sections, South China. Earth Planet. Sci. Lett. 305 (1–2), 21–31.
Pu, J.P., Bowring, S.A., Ramezani, J., Myrow, P., Raub, T.D., Landing, E., Mills, A., Hodgin, E., Macdonald, F.A., 2016. Dodging snowballs: geochronology of the Gaskiers glaciation and the first appearance of the Ediacaran biota. Geology 44, 955–958.
Qin, S., Li, F., Zhou, Z., Zhou, G., 2018. Geochemical characteristics of water-dissolved gases and implications on gas origin of Sinian to Cambrian reservoirs of Anyue gas field in Sichuan Basin, China. Mar. Pet. Geol. 89, 83–90.
Ren, R., Guan, S., Wu, L., Zhu, G., 2018. Evolution of the Neoproterozoic rift basins and its implication for oil and gas exploration in the Tarim Basin. Petrol. Res. 3, 66–76.
Ren, R., Guan, S., Zhang, S., Wu, L., Zhang, H., 2020. How did the peripheral subduction drive the Rodinia breakup: constraints from the Neoproterozoic tectonic process in the northern Tarim Craton. Precambrian Res. 339, 1–17.
Sahoo, S.K., Planavsky, N.J., Kendall, B., Wang, X., Shi, X., Scott, C., Anbar, A.D., Lyons, T.W., Jiang, G., 2012. Ocean oxygenation in the wake of the Marinoan glaciation. Nature 489, 546–549.
Sawaki, Y., Ohno, T., Tahata, M., Komiya, T., Hirata, T., Maruyama, S., Windley, B.F., Han, J., Shu, D., Li, Y., 2010. The Ediacaran radiogenic Sr isotope excursion in the Doushantuo Formation in the Three Gorges Area, South China. Precambrian Res. 176 (1–4), 46–64.
Scheller, E.L., Dickson, A.J., Canfield, D.E., Korte, C., Kristiansen, K.K., Dahl, T.W., 2018. Ocean redox conditions between the snowballs – geochemical constraints from Arena Formation, East Greenland. Precambrian Res. 319, 173–186.
Shen, W., Zhu, X., Xie, H., Wang, X., He, Y., 2022. Tectonic–sedimentary evolution during initiation of the Tarim Basin: Insights from late Neoproterozoic sedimentary records in the NW basin. Precambrian Res. 371, 106598.
Shi, K., Liu, B., Tian, J., Pan, W., 2016. Sedimentary characteristics and lithofacies paleogeography of Sinian in Tarim Basin. Acta Pet. Sin. 37 (11), 1343–1360.
Shi, K., Liu, B., Liu, H., Liu, J., Pan, W., 2017. Neoproterozoic tectono-sedimentary evolution in Quruqtagh area, NE Tarim Basin, Xinjiang, China. Earth Sci. Front. 24 (1), 297–307.
Shu, L.S., Deng, X.L., Ma, D.S., Xiao, W.J., 2011. Precambrian tectonic evolution of the Tarim Block, NW China: new geochronological insights from the Quruqtagh domain. J. Asian Earth Sci. 42, 774–790.
Sun, D., Li, S., Li, J., Li, Y., Yang, T., Feng, X., Li, H., Han, Z., He, Z., 2022. Insights from a comparison of hydrocarbon accumulation conditions of Sinian-Cambrian between the Tarim and the Sichuan basins. Acta Geol. Sin. 96 (1), 249–264.
Tang, Q.Y., Zhang, Z.W., Li, C., Wang, Y.L., Ripley, E.M., 2016. Neoproterozoic subduction-related basaltic magmatism in the northern margin of the Tarim Craton: implications for Rodinia reconstruction. Precambrian Res. 286, 370–378.
Thompson and Bowring, 2000. Age of the squantum "Tillite" Boston Basin, Massachusetts: U-Pb zircon constraints on terminal Neoproterozoic Glaciation. Am. J. Sci. 300, 630–655.
Turner, S.A., 2010. Sedimentary record of late Neoproterozoic rifting in the NW Tarim Basin China. Precambrian Res. 181, 85–96.
Vandyk, T.M., Wu, G., Davies, B.J., Xiao, Y., Li, M., Shields, G.A., Le Heron, D.P., 2019. Temperate glaciation on a Snowball Earth: glaciological and palaeogeographic insights from the Cryogenian Yuermeinak Formation of NW China. Precambrian Res. 331, 105362.
Wang, J., Li, Z.X., 2003. History of Neoproterozoic rift basins in South China: implications for Rodinia break up. Precambrian Res. 122, 141–158.
Wang, A.G., Zhang, C.L., Zhao, Y., 2004. Depositional types of the lower part of the Nanhua system at the southwestern margin of Tarim and their tectonic significance. J. Stratigr. 28, 248–256.
Wang, C., Wang, Y.H., Liu, L., He, S.P., Li, R.S., Li, M., Yang, W.Q., Cao, Y.-T., Meert, J. G., Shi, C., 2014. The Paleoproterozoic magmatic–metamorphic events and cover sediments of the Tiekelik Belt and their tectonic implications for the southern margin of the Tarim Block, northwestern China. Precambrian Res. 254, 210–225.
Wang, P., Algeo, T.J., Zhou, Q., Yu, W., Du, Y., Qin, Y., Xu, Y., Yuan, L., Pan, W., 2019. Large accumulations of ^{34}S-enriched pyrite in a low-sulfate marine basin: the Sturtian Nanhua Basin, South China. Precambrian Res. 335, 105504.
Wang, P., Du, Y., Yu, W., Algeo, T.J., Zhou, Q., Xu, Y., Qi, L., Yuan, L., Pan, W., 2020a. The chemical index of alteration (CIA) as a proxy for climate change during glacial-interglacial transitions in Earth history. Earth Sci. Rev. 201, 103032.
Wang, P., Zhao, G., Liu, Q., Han, Y., Yao, J., Li, J., 2020b. Zircons from the Tarim basement provide insights into its positions in Columbia and Rodinia supercontinents. Precambrian Res. 341, 105621.
Wei, G., Yang, W., Zhang, J., Xie, W., Zeng, F., Su, N., Jin, H., 2018. The pre-Sinian rift in central Sichuan Basin and its control on hydrocarbon accumulation in the overlying strata. Pet. Explor. Dev. 45 (2), 179–189.
Wei, G., Wei, W., Wang, D., Li, T., Yang, X., Shields, G.A., Zhang, F., Li, G., Chen, T., Yang, T., Ling, H., 2020. Enhanced chemical weathering triggered an expansion of euxinic seawater in the aftermath of the Sturtian glaciation. Earth Planet. Sci. Lett. 539, 1–12.
Wen, B., Evans, D.A.D., Wang, C., Li, Y.X., Jing, X.Q., 2018. A positive test for the Greater Tarim Block at the heart of Rodinia: mega-dextral suturing of supercontinent assembly. Geology 46, 687–690.
Wu, G.H., Zhang, C.Z., Wang, H., Liu, Y.K., Li, J.J., 2009. Zircon SHRIMP U-Pb age of granodiorite of the Tacan 1 well in the central Tarim basin, China. Geol. Bull. China 28, 568–571.
Wu, G.H., Chen, Z.Y., Qu, Y.L., Zhang, C.Z., 2012. SHRIMP zircon age of the high aeromagnetic anomaly zone in central Tarim Basin and its geological implications. Nat. Sci. 4, 1–4.
Wu, L., Guan, S., Yang, H., Ren, R., Zhu, G., Jin, J., Zhang, C., 2017. The paleogeographic framework and hydrocarbon exploration potential of Neoproterozoic rift basin in northern Tarim Basin. Acta Pet. Sin. 38, 375–385.
Wu, L., Guan, S., Zhang, S., Yang, H., Jin, J., Zhang, X., Zhang, C., 2018a. Neoproterozoic stratigraphic framework of the Tarim Craton in NW China: implications for rift evolution. J. Asian Earth Sci. 158, 240–252.

Wu, G., Xiao, Y., Bonin, B., Ma, D., Li, X., Zhu, G., 2018b. Ca. 850 Ma magmatic events in the Tarim Craton: age, geochemistry and implications for assembly of Rodinia supercontinent. Precambrian Res. 305, 489–503.
Wu, L., Guan, S., Feng, X., Ren, R., Zhang, C., 2020a. Discussion on stratigraphic division of the Nanhuan and Sinian of the Tarim Basin and its surrounding regions. Acta Petrol. Sin. 36, 3427–3441.
Wu, G., Yang, S., Meert, J., Xiao, Y., Chen, Y., Wang, Z., Li, X., 2020b. Two phases of Paleoproterozoic orogenesis in the Tarim Craton: implications for Columbia assembly. Gondwana Res. 83, 201–216.
Wu, G., Yang, S., Liu, W., Nance, R.D., Chen, X., Wang, Z., Xiao, Y., 2021a. Switching from advancing to retreating subduction in the Neoproterozoic Tarim Craton, NW China: implications for Rodinia breakup. Geosci. Front. 12, 161–171.
Wu, L., Zhu, G., Yan, L., Feng, X., Zhang, Z., 2021b. Late Ediacaran to early Cambrian tectonic–sedimentary controls on Lower Cambrian black shales in the Tarim Basin, Northwest China. Glob. Planet. Chang. 205, 103612.
Wu, L., Feng, X., Guan, S., Zhu, G., Yang, H., 2022a. Proterozoic basin–orogen framework in the northern Tarim Craton, China. Precambrian Res. 373, 106627.
Wu, H.X., Zhang, F.Q., Dilek, Y., Chen, H.L., Wang, C.Y., Lin, X.B., Cheng, X.G., Zhu, K. Y., 2022b. Mid–Neoproterozoic collision of the Tarim Craton with the Yili–Central Tianshan Block towards the final assembly of Supercontinent Rodinia: A new model. Earth Sci. Rev. 228, 103989.
Wu, H.-X., Dilek, Y., Zhang, F.-Q., Chen, H.-L., Chen, H., Wang, C.-Y., Lin, X.-B., Cheng, X.-G., 2023. Ediacaran magmatism and rifting along the northern margin of the Tarim craton: Implications for the late Neoproterozoic Rodinia configuration and breakup. GSA Bull. 135 (1–2), 367–388.
Xiao, S.H., Bao, H.M., Wang, H.F., Kaufman, A.J., Zhou, C.M., Li, G.X., Yuan, X.L., Ling, H.F., 2004. The Neoproterozoic Quruqtagh Group in eastern Chinese Tianshan: evidence for a post-Marinoan glaciation. Precambrian Res. 130 (1–4), 1–26.
Xie, Z., Wei, G., Zhang, J., Yang, W., Zhang, L., Wang, Z., Zhao, J., 2017. Characteristics of source rocks of the Datangpo Fm, Nanhua System, at the southeastern margin of Sichuan Basin and their significance to oil and gas exploration. Nat. Gas Ind. 4 (6), 405–414.
Xu, B., Jiang, P., Zheng, H.F., Zou, H.B., Zhang, L.F., Liu, D.Y., 2005. U-Pb zircon geochronology of Neoproterozoic volcanic rocks in the Tarim Block of northwest China: implications for the breakup of Rodinia supercontinent and Neoproterozoic glaciations. Precambrian Res. 136, 107–123.
Xu, B., Xiao, S.H., Zou, H.B., Chen, Y., Li, Z.X., Song, B., Liu, D.Y., Zhou, C.M., Yuan, X.L., 2009. SHRIMP zircon U-Pb age constraints on Neoproterozoic Quruqtagh diamictites in NW China. Precambrian Res. 168, 247–258.
Xu, Z.Q., He, B.Z., Zhang, C.L., Zhang, J.X., Wang, Z.M., Cai, Z.H., 2013a. Tectonic framework and crustal evolution of the Precambrian basement of the Tarim Block in NW China: new geochronological evidence from deep drilling samples. Precambrian Res. 235, 150–162.
Xu, B., Zou, H.B., Chen, Y., He, J.Y., Wang, Y., 2013b. The Sugetbrak basalts from northwestern Tarim Block of northwest China: geochronology, geochemistry and implications for Rodinia breakup and ice age in the Late Neoproterozoic. Precambrian Res. 236, 214–226.
Yan, L., Zhu, G., Chen, Y., Han, C., Yang, M., Du, D., Zhu, W., 2019. Distribution of lower Cambrian source rocks in the Tarim Basin. Nat. Gas Geosci. 30, 1569–1578.
Yan, L., Wei, G., Zhu, G., Chen, Y., Luo, C., Yang, M., Wang, S., Du, D., 2022. Exploration field analysis and zone optimization of Sinian, Tarim Basin. Nat. Gas Geosci. 33 (4), 548–555.
Yang, H.Q., Luo, C.Y., Zhu, B.Q., Zhang, K.C., 1997. The geological features and metallogenetic conditions of the copper-nickel-bearing basic-ultrabasic intrusion in Xingdi, Xinjiang. Northwest Geosci. 18, 43–53.
Yang, H.J., Wu, G.H., Kusky, T.M., Chen, Y.Q., Xiao, Y., 2018. Paleoproterozoic assembly of the North and South Tarim terranes: new insights from deep seismic profiles and Precambrian granite cores. Precambrian Res. 305, 151–165.
Yang, H., Deng, X., Zhang, Y., Xie, Z., Li, Y., Li, S., Zhang, H., Zhu, Y., Chen, Y., 2020. Great discovery and its significance of exploration for Ordovician ultra-deep fault-controlled carbonate reservoirs of Well Manshen 1 in Tarim Basin. China Petrol. Explor. 25 (3), 13–23.
Ye, X.T., Zhang, C.L., 2020. Advances in Meso- to Neoproterozoic stratigraphy of the Southwestern Tarim. Geol. Survey Res. 43, 161–168.
Ye, H.-M., Li, X.-H., Lan, Z.-W., 2013. Geochemical and Sr–Nd–Hf–O–C isotopic constraints on the origin of the Neoproterozoic Qieganbulake ultramafic–carbonatite complex from the Tarim Block, Northwest China. Lithos 182–183, 150–164.
Yi, Z., Guo, Z., Wei, G., 2022. A two-stage plume-induced rifting in the Neoproterozoic North Tarim: evidence from detrital zircon study and seismic interpretation. Tectonophysics 838, 229503.
Yong, W., Zhang, L., Hall, C.M., Mukasa, S.B., Essene, E.J., 2013. The $^{40}Ar/^{39}Ar$ and Rb–Sr chronology of the Precambrian Aksu blueschists in western China. J. Asian Earth Sci. 63, 197–205.
Yonkee, W.A., Dehler, C.D., Link, P.K., Balgord, E.A., Keeley, J.A., Hayes, D.S., Wells, M. L., Fanning, C.M., Johnston, S.M., 2014. Tectono-stratigraphic framework of Neoproterozoic to Cambrian strata, west-central US: protracted rifting, glaciation, and evolution of the North American Cordilleran margin. Earth Sci. Rev. 136, 59–95.
Yuan, C., Sun, M., Yang, J.S., Zhou, H., Zhou, M.F., 2004. Nb-depleted, continental rift-related Akaz metavolcanic rocks (West Kunlun): implication for the rifting of the Tarim Block from Gondwana. Geological Society. Special Publication, London 226, 131–143.
Zhai, M., 2013. The main old lands in China and assembly of Chinese unified continent. Sci. China Earth Sci. 56, 1829–1852.
Zhai, M.G., Santosh, M., Zhang, L.C., 2011. Precambrian geology and tectonic evolution of the North China Craton. Gondwana Res. 20 (1), 1–5.
Zhang, C.L., Li, X.H., Li, Z.X., Lu, S.N., Ye, H.M., Li, H.M., 2007a. Neoproterozoic ultramfic-mafic-carbonatite complex and granitoids in Quruqtagh of northeastern Tarim Block, western China: geochronology, geochemistry and tectonic implications. Precambrian Res. 152, 149–169.
Zhang, C.L., Li, Z.X., Li, X.H., Ye, H.M., 2007b. Early Palaeoproterozoic high-K intrusive complex in southwestern Tarim Block, NW China: age, geochemistry and implications for the Paleoproterozoic tectonic evolution of Tarim. Gondwana Res. 12, 101–112.
Zhang, C.L., Li, Z.X., Li, X.H., Ye, H.M., 2009a. Neoproterozoic mafic dyke swarm in north margin of the Tarim, NW China: age, geochemistry, petrogenesis and tectonic implications. J. Asian Earth Sci. 35, 167–179.
Zhang, Z.Y., Zhu, W.B., Shu, L.S., Su, J.B., Zheng, B.H., 2009b. Neoproterozoic ages of the Kuluketage diabase dyke swarm in Tarim, NW China, and its relationship to the breakup of Rodinia. Geol. Mag. 146, 150–154.
Zhang, Z.Y., Zhu, W.B., Shu, L.S., Wan, J.L., Yang, W., Su, J.B., Zheng, B.H., 2009c. Apatite fission track thermochronology of the Precambrian Aksu blueschist, NW China: Implications for thermo–tectonic evolution of the north Tarim basement. Gondwana Res. 16, 182–188.
Zhang, C.L., Yang, D.S., Wang, H.Y., 2010. Neoproterozoic mafic dyke swarm and basalt in southern margin of the Tarim Block: age, geochemistry and their geodynamic implications. Acta Geol. Sin. 84, 549–562.
Zhang, Y., Wang, Z., Yan, Z., Wang, T., 2011a. Tectonic setting of Neoproterozoic Beiyixi formation in Quruqtagh area, Xinjiang: evidence from geochemistry of clastic rocks. Acta Petrol. Sin. 27 (6), 1785–1796.
Zhang, C.L., Yang, D.S., Wang, H.Y., Takahashi, Y., Ye, H.M., 2011b. Neoproterozoic ultramfic-mafic layered intrusion in Quruqtagh of northeastern Tarim Block, NW China: two phases of mafic igneous activity of different mantle sources. Gondwana Res. 19, 177–190.
Zhang, C.L., Li, H., Santosh, M., Li, Z., Zou, H., Wang, H., Ye, H., 2012a. Precambrian evolution and cratonization of the Tarim Block, NW China: petrology, geochemistry, Nd-isotopes and U–Pb zircon geochronology from Archaean gabbro-TTG-potassic granite suite and Paleoproterozoic metamorphic belt. J. Asian Earth Sci. 47, 5–20.
Zhang, C.L., Zou, H.B., Li, H.K., Wang, H.Y., 2012b. Multiple phases of Neoproterozoic ultramafic-mafic complex in Kuruqtagh, northern margin of Tarim: interaction between plate subduction and mantle plume? Precambrian Res. 222–223, 488–502.
Zhang, C.L., Zou, H.B., Li, H.K., 2013. Tectonic framework and evolution of the Tarim Block, NW China. Gondwana Res. 23, 1306–1315.
Zhang, C.L., Zou, H.B., Santosh, M., Ye, X.T., Li, H.K., 2014a. Is the Precambrian basement of the Tarim Block in NW China composed of discrete terranes? Precambrian Res. 254, 226–244.
Zhang, J., Zhang, C.L., Li, H.K., Ye, X.T., Geng, J.X., Zhou, H.Y., 2014b. Revisit to time and tectonic environment of the Aksu blueschist terrane in northern Tarim, NW China: new evidence from zircon U-Pb age and Hf isotope. Acta Petrol. Sin. 30, 3357–3365.
Zhang, C.L., Ye, X.T., Zou, H.B., Chen, X.Y., 2016. Neoproterozoic sedimentary basin evolution in southwestern Tarim, NW China: new evidence from field observations, detrital zircon U-Pb ages and Hf isotope compositions. Precambrian Res. 280, 31–45.
Zhang, J., Yu, S., Mattinson, C., 2017. Early Paleozoic polyphase metamorphism in northern Tibet, China. Gondwana Res. 41, 267–289.
Zhang, C.L., Li, H.K., Ernst, R., Liu, X.Q., Zhong, Y., Zhang, J., 2019a. A fragment of the ca. 890 Ma large igneous province (LIP) in southern Tarim, NW China: a missing link between São Francisco, Congo and North China cratons. Precambrian Res. 333, 105428.
Zhang, C., Ye, X., Ernst, R.E., Zhong, Y., Zhang, J., Li, H., Long, X., 2019b. Revisiting the Precambrian evolution of the Southwestern Tarim terrane: implications for its role in Precambrian supercontinents. Precambrian Res. 324, 18–31.
Zhang, C.L., Zou, H.B., Ye, X.T., Chen, X.Y., 2019c. Tectonic evolution of the West Kunlun Orogenic Belt along the northern margin of the Tibetan Plateau: implications for the assembly of the Tarim terrane to Gondwana. Geosci. Front. 10, 973–988.
Zhang, Z., Zhu, G., Wu, G., Li, T., Feng, X., Jing, Y., 2022. Carbon isotopic chemostratigraphy of the Ediacaran-Cambrian successions in the northwestern Tarim Craton, NW China: correlations with Gondwana supercontinent. Glob. Planet. Chang. 208, 103702.
Zhao, G.C., Cawood, P.A., 2012. Precambrian geology of the North China, South China and Tarim Blocks. Precambrian Res. 222–223, 13–54.
Zhao, G., Wang, Y., Huang, B., Dong, Y., Li, S., Zhang, G., Yu, S., 2018. Geological reconstructions of the East Asian blocks: From the breakup of Rodinia to the assembly of Pangea. Earth-Sci. Rev. 186, 262–286.
Zhao, Y.Y., Zheng, Y.F., 2010. Record and time of Neoproterozoic glaciations on Earth. Acta Petrol. Sin. 27, 545–565.
Zhao, G.C., Li, S.Z., Sun, M., Wilde, S.A., 2011. Assembly, accretion, and break-up of the Palaeo-Mesoproterozoic Columbia supercontinent: records in the North China Craton revisited. Int. Geol. Rev. 53, 1331–1356.
Zhao, P., Chen, Y., Zhan, S., Xu, B., Faure, M., 2014. The Apparent Polar Wander Path of the Tarim block (NW China) since the Neoproterozoic and its implications for a long-term Tarim-Australia connection. Precambrian Res. 242, 39–57.
Zheng, Y.F., Wu, Y.B., Gong, B., Chen, R.X., Tang, J., Zhao, Z.F., 2007. Tectonic driving of Neoproterozoic glaciations: evidence from extreme oxygen isotope signature of meteoric water in granite. Earth Planet. Sci. Lett. 256, 196–210.
Zheng, Y.F., Xiao, W.J., Zhao, G.C., 2013. Introduction to tectonics of China. Gondwana Res. 23, 1189–1206.
Zhou, C., Tucker, R., Xiao, S., Peng, Z., Yuan, X., Chen, Z., 2004. New constraints on the ages of Neoproterozoic glaciations in South China. Geology 32, 437–440.
Zhou, X., Li, J., Fu, C., Li, W., Wang, H., 2012. Discussions on the Cryogenian-Cambrian tectonic-sedimentary event and tectonic setting of northern Tarim Basin. Geol. China 39 (4), 900–910.

Zhou, T., Ge, R., Zhu, W., Wu, H., 2021. Is there a Grenvillian orogen in the southwestern Tarim Craton? Precambrian Res. 354, 106053.
Zhou, X., Tian, W., Wu, G., Damian Nance, R., Chen, Y., Zhao, Y., Yan, W., Zhang, Y., 2022. Geochemistry and U-Pb-Hf zircon systematics of Cryogenian syn-rift magmatic rocks from the subsurface of the Tarim Craton: implications for subduction-related continental rifting. Precambrian Res. 377, 106733.
Zhu, G., Zhang, Z., Jiang, H., Yan, L., Chen, W., Li, T., Li, X., 2023b. Evolution of the Cryogenian cratonic basins in China, paleo-oceanic environment and hydrocarbon generation mechanism of ancient source rocks, and exploration potential in 10,000 m-deep strata. Earth-Sci. Rev. 244, 104506.
Zhu, W.B., Zhang, Z.Z., Shu, L.S., Lu, H.F., Sun, J.B., Yang, W., 2008. SHRIMP U–Pb zircon geochronology of Neoproterozoic Korla mafic dykes in the northern Tarim Block, NW China: implications for the long-lasting breakup process of Rodinia. J. Geol. Soc. Lond. 165, 887–890.
Zhu, W.B., Zheng, B.H., Shu, L.S., Ma, D.S., Wu, H.L., Li, Y.X., Huang, W.T., Yu, J.J., 2011. Neoproterozoic tectonic evolution of the Precambrian Aksu blueschist terrane, northwestern Tarim, China: insights from LA-ICP-MS zircon U-Pb ages and geochemical data. Precambrian Res. 185 (3), 215–230.
Zhu, G., Chen, F., Chen, Z., Zhang, Y., Xing, X., Tao, X., Ma, D., 2016. Discovery and basic characteristics of the high-quality source rocks of the Cambrian Yuertusi Formation in Tarim Basin. Nat. Gas Geosci. 27 (01), 8–21.
Zhu, G., Chen, F., Wang, M., Zhang, Z., Ren, R., Wu, L., 2018. Discovery of the lower Cambrian high-quality source rocks and deep oil and gas exploration potential in the Tarim Basin, China. AAPG Bull. 102, 2123–2151.
Zhu, G., Li, T., Zhao, K., Zhang, Z., Chen, W., Yan, H., Zhang, K., Chi, L., 2019. Excellent source rocks discovered in the Cryogenian interglacial deposits in South China: geology, geochemistry, and hydrocarbon potential. Precambrian Res. 333, 105455.
Zhu, G., Li, X., Li, T., Zhou, L., Wu, Y., Shen, B., Ning, M., 2023a. Genesis mechanism and Mg isotope difference between the Sinian and Cambrian dolomites in Tarim Basin. Sci. China Earth Sci. 66 (2), 334–357.
Zhu, G., Li, T., Zhang, Z., Zhao, K., Zhang, K., Chen, W., Yan, H., Wang, P., 2020a. Distribution and geodynamic setting of the Late Neoproterozoic–Early Cambrian hydrocarbon source rocks in the South China and Tarim Blocks. J. Asian Earth Sci. 201, 104504.
Zhu, G., Yan, H., Chen, W., Yan, L., Chen, Z., Li, T., Sun, Q., Xie, X., 2020b. Geochemical characteristics, formation and distribution of the Nanhua-Cambrian black rock series in the eastern Tarim Basin. Acta Petrol. Sin. 36, 3442–3462.
Zhu, G., Yan, H., Chen, W., Yan, L., Zhang, K., Li, T., Chen, Z., Wu, G., Santosh, M., 2020c. Discovery of Cryogenian interglacial source rocks in the northern Tarim, NW China: implications for Neoproterozoic paleoclimatic reconstructions and hydrocarbon exploration. Gondwana Res. 80, 370–384.
Zhu, G., Chen, Z., Chen, W., Yan, H., Zhang, P., 2021a. Revisiting to the Neoproterozoic tectonic evolution of the Tarim Block, NW China. Precambrian Res. 352, 106013.
Zhu, G., Liu, W., Wu, G., Ma, B., Nance, R.D., Wang, Z., Xiao, Y., Chen, Z., 2021b. Geochemistry and U-Pb-Hf detrital zircon geochronology of metamorphic rocks in terranes of the West Kunlun Orogen: protracted subduction in the northernmost Proto-Tethys Ocean. Precambrian Res. 363, 106344.
Zhu, G., Milkov, A.V., Li, J., Xue, N., Chen, Y., Hu, J., Li, T., Zhang, Z., Chen, Z., 2021c. Deepest oil in Asia: Characteristics of petroleum system in the Tarim basin, China. J. Pet. Sci. Eng. 199, 108246.
Zhu, G., Chen, W., Yan, H., Yan, L., Zhang, Z., Zhao, K., Li, T., 2022a. Sinian tectonic evolution and distribution of source rocks in Northwest Tarim Basin, China. Mar. Pet. Geol. 144, 105826.
Zhu, G., Hu, J., Chen, Y., Xue, N., Zhao, K., Zhang, Z., Li, T., Chen, Z., 2022b. Geochemical characteristics and formation environment of source rock of the lower Cambrian Yuertusi Formation in well Luntan 1 in Tarim Basin. Acta Geol. Sin. 96 (6), 2116–2130.
Zuza, A.V., Yin, A., 2017. Balkatach hypothesis: a new model for the evolution of the Pacific, Tethyan, and Paleo-Asian oceanic domains. Geosphere 13, 1664–1712.